## Finite Element Analysis and In Vitro Assessment of Multirooted Custom Implants Manufactured by Additive and Subtractive Technologies

Doctoral thesis

to obtain a doctorate (MD/PhD)

from the Faculty of Medicine

of the University of Bonn

## Mostafa Adel Mohamed Aldesoki Mohamed

from Cairo, Egypt 2025

Written with authorization of the University of Bonn
First reviewer: UnivProf. Dr.rer.nat. Christoph Peter Bourauel Second reviewer: Prof. Dr. Friedhelm Heinemann
Day of oral examination: 17.09.2025
From the Policlinic for Dental Prosthetics, Propaedeutics and Materials Science at the University of Bonn
Oral Technology

## Dedication

To the memory of my beloved mother, to my father for his unwavering support, to my siblings for their constant encouragement, to my wonderful wife for her love and patience, and to my son who fills my life with joy, with deepest gratitude and love.

Mostafa Aldesokí

## **Table of Contents**

	List of Abbreviations	6
1.	Abstract	7
2.	Introduction and Aims with References	8
	2.1 Introduction	8
	2.2 Aim of the Study	9
	2.3 References	10
3.	Publications	13
	3.1 Study 1	13
	3.2 Study 2	24
	3.3 Study 3	34
4.	Discussion with References	45
	4.1 Discussion	45
	4.2 Conclusions	47
	4.3 References	48
5.	Acknowledgements	51

## **List of Abbreviations**

AM Additive Manufacturing

CAD/CAM Computer-Aided Design/Computer-Aided Manufacturing

CBCT Cone-Beam Computed Tomography

CNC Computer Numerical Control

FEA Finite Element Analysis

LCM Lithography-Based Ceramic Manufacturing

MT Milled Titanium

MZ Milled Zirconia

PT 3D-Printed Titanium

PZ 3D-Printed Zirconia

RAI Root Analogue Implant

RMS Root Mean Square

SLM Selective Laser Melting

SM Subtractive Manufacturing

TI Threaded Implant

#### 1. Abstract

Objective: The aim of this study was to evaluate the accuracy of milled and 3D printed titanium and zirconia multi-rooted root analogue implants (RAIs) and compare their biomechanical behaviour to conventional threaded implants (TIs) experimentally and numerically through the creation of a validated finite element model. Materials and methods: A multi-rooted RAI was modelled based on tooth 47 segmented from cone-beam computed tomography (CBCT). Four RAI subgroups, 3D-printed titanium (PT), 3D-printed zirconia (PZ), milled titanium (MT), and milled zirconia (MZ), were fabricated, along with two TI subgroups (4.5 x 11 mm and 5.5 x 11 mm) as controls. Specimens were evaluated for precision and trueness using high-resolution scanning and 3D measurement software, with root mean square (RMS) deviations statistically analysed. Samples were embedded in artificial bone blocks and subjected to biomechanical testing using a specialised biomechanical test system to quantify micromotion. Additionally, a validated finite element model incorporating RAIs and TIs was developed, reproducing experimental boundary conditions. The model was assessed under immediate placement (touching contact) and osseointegrated conditions (glued contact). A 300 N load was applied axially and at 30° to evaluate equivalent stress, maximum principal stress, microstrain, and displacement. Re**sults:** PZ demonstrated the highest precision (RMS: 21±6 μm), while MZ had the highest trueness (RMS: 66±3 µm). MT exhibited the lowest trueness and the greatest deviation in the furcation area (612±64 µm). In vitro micromotion analysis showed no significant differences in the loading direction (Z-axis) between RAIs and TIs, whereas RAIs had higher total displacement compared to TIs (96.5 µm vs. 55.8 µm). Finite element analysis (FEA) showed that RAIs outperformed TIs, exhibiting lower stress, reduced microstrain (4,000 με vs. 13,000 με), and enhanced primary and secondary stability with lower micromotion. Conclusion: The manufacturing method significantly affected RAI accuracy, with PZ showing the highest precision and MZ the highest trueness. RAIs demonstrated promising biomechanical behaviour, though anatomical variations influenced predictability. FEA confirmed RAIs' superior stress distribution and stability over TIs, highlighting their potential as a viable alternative for immediate implant placement.

**Keywords:** Root Analogue Implant; Dental Implant; Accuracy; Biomechanics; Finite Element Analysis; 3D Printing.

#### 2. Introduction and Aims with References

#### 2.1 Introduction

Dental implants are a well-established treatment for replacing missing teeth, with a reported success rate of approximately 95 % after ten years (Moraschini et al., 2015). Immediate implant placement, in which the implant is inserted directly into the extraction socket, offers advantages such as reduced surgical interventions, lower costs, and shorter treatment duration (Beagle, 2006; Figliuzzi et al., 2012; Koh et al., 2010). However, challenges such as discrepancies between the extraction socket and conventional threaded implants (TIs) can lead to difficulties in positioning and reduced primary stability (Regish et al., 2013; Saeidi Pour et al., 2019; Yong, 2012).

Advancements in digital dentistry, particularly cone beam computed tomography (CBCT) and computer-aided design/computer-aided manufacturing (CAD/CAM), have enabled the fabrication of patient-specific root analogue implants (RAIs, Ghuneim, 2013; Moin et al., 2018; Regish et al., 2013). Designed to replicate the extracted tooth's root anatomy, RAIs achieve an optimal fit within the socket, potentially enhancing primary stability, reducing marginal bone loss, and simplifying placement compared to TIs (Anssari Moin et al., 2017; Chen et al., 2014; Mangano et al., 2014). Despite these advantages, challenges such as high manufacturing costs, complex fabrication, and limited clinical data remain significant concerns (Moin et al., 2013; 2018).

RAIs can be fabricated using either subtractive manufacturing (SM) or additive manufacturing (AM) (Dantas et al., 2021). SM, primarily through computer numerical control (CNC) milling, offers high precision and superior mechanical properties, particularly with 5-axis machines that enable complex geometries (Beuer et al., 2008; Bosch et al., 2014). However, milling is costly, time-consuming, and generates significant material waste, while tool wear can compromise accuracy (Jeong et al., 2018; Lerner et al., 2021).

Conversely, AM, particularly 3D printing, minimises material waste and allows for the efficient production of complex geometries with high accuracy (Revilla-León and Özcan, 2019; Zhang et al., 2019). Technologies such as lithography-based ceramic manufacturing (LCM) and selective laser melting (SLM) enable the fabrication of ceramic and metal

RAIs, respectively, but require additional post-processing steps like sintering or debinding (Schönherr et al., 2020; Schweiger et al., 2021). Despite these advancements, AM may still produce structures with lower density and mechanical strength compared to milling (Saeidi Pour et al., 2019).

Implant stability, defined as the absence of clinical mobility, is crucial for successful osseointegration (Ivanova et al., 2021; Sennerby and Meredith, 2008). It consists of primary
stability, achieved through mechanical anchorage upon insertion, and secondary stability,
which develops through bone remodelling and healing (Miri et al., 2017). While primary
stability is a mechanical property, secondary stability is a biological process influenced by
osseointegration. Factors such as implant geometry and bone quality play a critical role in
enhancing overall stability and long-term success (Figliuzzi et al., 2012; Ivanova et al.,
2021).

Finite element analysis (FEA) is a computational technique used to model complex physical structures by dividing them into smaller, interconnected elements (Lee and Lim, 2013). In dental research, FEA allows for the assessment of biomechanical behaviour in scenarios that are difficult to study experimentally. It also enables the evaluation of different materials and implant designs without additional costs (Aldesoki et al., 2022; Elshazly et al., 2023; Falcinelli et al., 2023 Wang et al., 2022).

#### 2.2 Aim of the Study

The aim of the current study was to:

- Assess the accuracy of multi-rooted titanium and zirconia RAIs fabricated using additive and subtractive techniques.
- 2. Experimentally analyse the micromotion of these RAIs by evaluating their load/displacement curves.
- 3. Develop a validated 3D finite element model based on experimental data to numerically investigate the biomechanical behaviour of multi-rooted RAIs.

#### 2.3 References

Aldesoki M, Bourauel C, Morsi T, El-Anwar MI, Aboelfadl AK, Elshazly TM. Biomechanical behavior of endodontically treated premolars restored with different endocrown designs: Finite element study. J Mech Behav Biomed Mater 2022; 133: 105309.

Anssari Moin D, Hassan B, Wismeijer D. A novel approach for custom three-dimensional printing of a zirconia root analogue implant by digital light processing. Clin Oral Implants Res 2017; 28: 668–670.

Beagle JR. The Immediate Placement of Endosseous Dental Implants in Fresh Extraction Sites. Dent Clin North Am 2006; 50: 375–389.

Beuer F, Schweiger J, Edelhoff D. Digital dentistry: An overview of recent developments for CAD/CAM generated restorations. Br Dent J 2008; 204: 505–511.

Bosch G, Ender A, Mehl A. A 3-dimensional accuracy analysis of chairside CAD/CAM milling processes. J Prosthet Dent 2014; 112: 1425–1431.

Chen J, Zhang Z, Chen X, Zhang C, Zhang G, Xu Z. Design and manufacture of customized dental implants by using reverse engineering and selective laser melting technology. J Prosthet Dent 2014; 112: 1088–1095.E1.

Dantas T, Madeira S, Gasik M, Vaz P, Silva F. Customized root-analogue implants: A review on outcomes from clinical trials and case reports. Materials (Basel) 2021; 14: 1–14.

Elshazly TM, Bourauel C, Aldesoki M, Ghoneima A, Abuzayda M, Talaat W, Talaat S, Keilig L. Computer-aided finite element model for biomechanical analysis of orthodontic aligners. Clin Oral Investig 2023; 27: 115–124.

Falcinelli C, Valente F, Vasta M, Traini T. Finite element analysis in implant dentistry: State of the art and future directions. Dent Mater 2023; 39: 539–556.

Figliuzzi M, Mangano F, Mangano C. A novel root analogue dental implant using CT scan and CAD/CAM: Selective laser melting technology. Int J Oral Maxillofac Surg 2012; 41: 858–862.

Ghuneim WA. In situ tooth replica custom implant: A 3-dimensional finite element stress and strain analysis. J Oral Implantol 2013; 39: 559–573.

Ivanova V, Chenchev I, Zlatev S, Mijiritsky E. Correlation between primary, secondary stability, bone density, percentage of vital bone formation and implant size. Int J Environ Res Public Health 2021; 18.

Jeong YG, Lee WS, Lee KB. Accuracy evaluation of dental models manufactured by CAD/CAM milling method and 3D printing method. J Adv Prosthodont 2018; 10: 245–251.

Koh RU, Rudek I, Wang HL. Immediate implant placement: Positives and negatives. Implant Dent 2010; 19: 98–108.

Lee JS, Lim YJ. Three-dimensional numerical simulation of stress induced by different lengths of osseointegrated implants in the anterior maxilla. Comput Methods Biomech Biomed Engin 2013; 16: 1143–1149.

Lerner H, Nagy K, Pranno N, Zarone F, Admakin O, Mangano F. Trueness and precision of 3D-printed versus milled monolithic zirconia crowns: An in vitro study. J Dent 2021; 113: 103792.

Mangano FG, De Franco M, Caprioglio A, MacChi A, Piattelli A, Mangano C. Immediate, non-submerged, root-analogue direct laser metal sintering (DLMS) implants: A 1-year prospective study on 15 patients. Lasers Med Sci 2014; 29: 1321–1328.

Miri R, Shirzadeh A, Kermani H, Khajavi A. Relationship and changes of primary and secondary stability in dental implants: A review. Int J Contemp Dent Med Rev 2017; 6.

Moin DA, Hassan B, Mercelis P, Wismeijer D. Designing a novel dental root analogue implant using cone beam computed tomography and CAD/CAM technology. Clin Oral Implants Res 2013; 24: 25–27.

Moin D, Hassan B, Wismeijer D. Immediate nonsubmerged custom root analog implants: A prospective pilot clinical study. Int J Oral Maxillofac Implants 2018; 33: e37–e44. Moraschini V, Poubel LADC, Ferreira VF, Barboza EDSP. Evaluation of survival and success rates of dental implants reported in longitudinal studies with a follow-up period of at least 10 years: A systematic review. Int J Oral Maxillofac Surg 2015; 44: 377–388.

Regish KM, Sharma D, Prithviraj DR. An overview of immediate root analogue zirconia implants. J Oral Implantol 2013; 39 (2): 225–233.

Revilla-León M, Özcan M. Additive manufacturing technologies used for processing polymers: Current status and potential application in prosthetic dentistry. J Prosthodont 2019; 28: 146–158.

Saeidi Pour R, Freitas Rafael C, Engler MLPD, Edelhoff D, Klaus G, Prandtner O, Berthold M, Liebermann A. Historical development of root analogue implants: A review of published papers. Br J Oral Maxillofac Surg 2019; 57: 496–504.

Schönherr JA, Baumgartner S, Hartmann M, Stampfl J. Stereolithographic additive manufacturing of high precision glass ceramic parts. Materials (Basel) 2020; 13: 1492.

Schweiger J, Edelhoff D, Güth JF. 3D printing in digital prosthetic dentistry: An overview of recent developments in additive manufacturing. J Clin Med 2021; 10: 2010.

Sennerby L, Meredith N. Implant stability measurements using resonance frequency analysis: Biological and biomechanical aspects and clinical implications. Periodontol 2000 2008; 47: 51–66.

Wang JQ, Zhang Y, Pang M, Wang YQ, Yuan J, Peng H, Zhang W, Dai L, Li HW. Biomechanical comparison of six different root-analog implants and the conventional Morse taper implant by finite element analysis. Front Genet 2022; 13: 1–11.

Yong LT. Single stage immediate implant placements in the esthetic zone. J Oral Implantol 2012; 38: 738–746.

Zhang ZC, Li PL, Chu FT, Shen G. Influence of the three-dimensional printing technique and printing layer thickness on model accuracy. J Orofac Orthop 2019; 80: 194–204.

## 3. Publications

## 3.1 Study 1

Trueness and precision of milled and 3D printed root-analogue implants:

A comparative in vitro study

Mostafa Aldesoki, Ludger Keilig, Istabrak Dörsam, Bernd Evers-Dietze, Tarek M. Elshazly, Christoph Bourauel

Journal of Dentistry (2023)

https://doi.org/10.1016/j.jdent.2023.104425

Impact factor: 4.8



Contents lists available at ScienceDirect

## Journal of Dentistry

journal homepage: www.elsevier.com/locate/jdent





## Trueness and precision of milled and 3D printed root-analogue implants: A comparative *in vitro* study

Mostafa Aldesoki <sup>a,\*</sup>, Ludger Keilig <sup>a,b</sup>, Istabrak Dörsam <sup>a,b</sup>, Bernd Evers-Dietze <sup>c</sup>, Tarek M. Elshazly <sup>a</sup>, Christoph Bourauel <sup>a</sup>

- a Oral Technology, Dental School, University Hospital Bonn, Bonn, Germany
- <sup>b</sup> Department of Prosthodontics, Dental School, University Hospital Bonn, Bonn, Germany
- <sup>c</sup> Department of Electrical Engineering, Mechanical Engineering and Technical Journalism (EMT), Bonn-Rhein-Sieg University of Applied Sciences, Sankt Augustin, Germany

#### ARTICLE INFO

## Keywords: Root analogue implant (RAI) Accuracy Precision Trueness 3D printing Milling

#### ABSTRACT

*Objectives*: The present study aimed to evaluate the accuracy (trueness and precision) of titanium and zirconia multi-rooted root analogue implants (RAIs) manufactured by milling and 3D-printing.

*Methods*: A multi-rooted RAI was designed based on a mandibular second molar segmented from cone-beam computed tomography (CBCT). The manufactured RAIs were divided into four groups: 3D-printed titanium (PT) and 3D-printed zirconia (PZ) (n=10 each), as well as milled titanium (MT) and milled zirconia (MZ) (n=5 each). The specimens were scanned with a high-precision scanner, and the scanned data were imported into 3D-measurement software to evaluate the precision and trueness of each group. Root mean square (RMS) deviations were measured and statistically analysed (One-way ANOVA, Tukey's,  $p \le 0.05$ ).

Results: PZ showed the highest precision with RMS value of  $21\pm6~\mu m$ . Nevertheless, there was no statistically significant difference in precision among the other groups. Regarding trueness, MZ showed the highest trueness with RMS value of  $66\pm3~\mu m$ , whereas MT showed the lowest trueness result. Inspection sections showed that MT had significantly high RMS deviation in the furcation area ( $612\pm64~\mu m$ ), whereas PZ showed significantly high RMS deviation at the apical area ( $197\pm17~\mu m$ ).

Conclusions: The manufacturing process significantly influenced the RAI accuracy. PZ exhibited the highest precision, whereas MZ exhibited the highest trueness, followed by PT. Finally, our results suggest that 3D-printing can reproduce concave surfaces and less accessible areas better than milling.

Clinical Significance: Milled and 3D-printed RAIs showed promising results in terms of precision and trueness. However, further clinical research is needed to advocate their use as immediate implants. Additionally, the inherent volumetric changes of the various materials during manufacturing should be considered.

#### 1. Introduction

Dental implants are considered a successful treatment modality for replacing missing teeth with a success rate of almost 95% after ten years [1]. Immediate implants are implants that are immediately inserted into the extraction socket of the tooth to be replaced [2,3]. The benefit of this immediate implant placement is that it reduces the number of surgical interventions, the cost, and the overall duration of treatment [4]. Although immediate implants offer many advantages, they are associated with some surgical challenges, such as difficult implant positioning and decreased primary stability caused by the shape discrepancy

between the socket and the conventional threaded implant [5–7].

Recent advances in computer-aided design/computer-aided manufacturing (CAD/CAM) technology combined with cone beam computed tomography (CBCT) rendered it possible to fabricate a customised patient-specific root analogue implant (RAI) as an alternative to threaded implants (TI) [5,8,9]. The design of the RAI is based on the root anatomy of the tooth to be extracted and therefore, unlike the threaded implant, fits perfectly into the empty socket without creating a discrepancy; this in turn should increase primary stability, reduce marginal bone loss, and make insertion less complicated [10–12].

RAIs are manufactured either by subtractive (milling) or additive

E-mail address: aldesoki@uni-bonn.de (M. Aldesoki).

 $<sup>^{\</sup>ast}$  Corresponding author.

(3D printing) manufacturing [13]. In subtractive manufacturing (SM), computer numerical control (CNC) milling machines are classified according to the number of axes into 3-axis, 4-axis, or 5-axis machines [14, 15]. A 5-axis machine can move linearly in the three spatial directions X, Y, and Z, as well as rotate around the A and B axes. The rotation is done either by the spindle or the workpiece, which allows milling of complex 3D geometries with extremely high accuracy [16,17]. However, this is more expensive than using the 3- or 4-axis machines and requires a longer machining time [16,18,19]. Although milling is the most widely used manufacturing process [18], it has many limitations, such as high material waste due to the unusable remnants of disks and blocks, high maintenance costs for the machine, and slow manufacturing process. In addition, milling burs are highly susceptible to wear, especially for fully sintered ceramics, and their size also affects the reproduction of the surface geometry and limits the ability to bypass deep undercuts [20-22].

To overcome the limitations of SM, additive manufacturing (AM) is now widely used in dentistry [23]. 3D printing is a CAM process that converts a digital model into a physical model through layer-by-layer material deposition [24,25]. It reduces material waste as only the support material needs to be disposed. It also enables the simultaneous production of multiple models in less time and can produce extremely complex geometries with high accuracy [11,20,21,23]. For these reasons, 3D printing is widely regarded as the future of RAIs [11].

One of the recent innovations in rapid prototyping technologies is 3D printing of advanced ceramics using lithography-based ceramic manufacturing (LCM). This technology is based on digital light processing (DLP) [26], in which a ceramic slurry coated with a photosensitive resin is activated using a light-emitting diode (LED) device [27]. Once the part is formed layer-by-layer by selective polymerization, it is called a green body. This green body requires further thermal treatment involving debinding and sintering. Debinding burns out the photopolymer network and organic components, whereas sintering densifies the ceramic particles by fusing them together [28,29]. Another type of AM is selective laser melting (SLM), in which powdered metal material is melted with a high-power fibre laser in an inert chamber. This laser beam melts each layer into the previous one until the solid body is formed from thousands of superimposed micro-welds [11,30,31].

According to the international organization for standardization (ISO 5725-1:1994), trueness refers to how close the measured values are to a reference value, whereas precision refers to how repeated measurements in the same group are close to each other, and both trueness and precision quantify the accuracy of a 3D model [32]. In several studies, the accuracy of milled and 3D printed dental models has been discussed [13,20,33,34], however, to our knowledge, few studies have evaluated the accuracy of RAIs [10,11,35]. Yet, the accuracy of multi-rooted RAIs, in particular, has not been discussed.

Hence, the aim of this study was to evaluate the accuracy of titanium and zirconia multi-rooted RAIs manufactured by additive and subtractive methods. The null hypothesis was that there would be no statistically significant difference in accuracy amongst the examined groups (p > 0.05).

#### 2. Methods

#### 2.1. Data acquisition and preparation of the RAI STL file

A CBCT scan of the mandible of a dentulous patient who was not identified by sex, age, or ethnic group was selected for the construction of the RAI 3D model. The equipment was adjusted to scan the entire tooth with a beam accelerating voltage of 90 kV and an X-ray beam current of 12 mA with a voxel dimension of 75  $\mu m$ . The total scanning time was 15 s, and a total of 668 slices were scanned for modelling.

Next, the CBCT scan was segmented using a 3D medical image processing software (Mimics 22; Materialise, Leuven, Belgium) whereby the mandibular right second molar (tooth 47) was segmented by assigning a minimum and a maximum threshold based on histogram analysis. Subsequently, the segmented tooth was exported to a 3D printing, design and remeshing software (3-matic 15; Materialise, Leuven, Belgium) to finalise the design of the RAI based on the anatomy of the tooth. Since the focus in our study was on the root-shaped portion of the implant, the coronal portion was designed as an idealised cube with a side length of 5 mm to facilitate further biomechanical investigations. The modelled RAI was then exported as a standard tessellation language (STL) file, which will serve as a reference model.

#### 2.2. Preparation of the milled and 3D printed models

Using the predesigned RAI STL file, the specimens were fabricated either by 3D printing or by milling, as shown in Table 1. Milling was performed with 5-axis CNC milling machines, placing the sprues on the idealised cube and on the mesial root of the RAI (Fig. 1A), whereas LCM and SLM technologies were used for the 3D printing of zirconia and titanium RAIs, respectively. The printing supports were placed on the overhanging coronal surface around the idealised cube. The RAIs were aligned upside down with the idealized cube facing the bed of the 3D printer, and the layer thickness was set to 25  $\mu$ m (Fig. 1B and 1C).

All produced RAIs were then scanned using the Atos Core industrial scanner (Atos Core 80; GOM GmbH, Braunschweig, Germany). Atos Core is a blue-light scanner with precise fringe patterns projected onto the surface of the object and captured by two cameras. This triple-scan principle can provide complete measurement data even for objects with indentations or reflective surfaces. The scanner unit was calibrated and tested according to VDI/VDIE 2634 (VDI e.V.; Düsseldorf, Germany) and had the following maximum deviations: 1  $\mu$ m probing error form (sigma), 2  $\mu$ m probing error (size), 2  $\mu$ m sphere spacing error, and 6  $\mu$ m length measurement error. A scanning spray (AESUB White; Scanning-spray Vertriebs GmbH, Recklinghausen, Germany) was applied to each sample before scanning to improve the scanning process specifically with the glossy surface of the titanium RAIs (Fig. 2A).

#### 2.3. Alignment and 3D analysis

All the scanned data were saved in STL format and imported into an evaluation software for the analysis of 3D measurement data (GOM Inspect Suite 2020; GOM GmbH, Braunschweig, Germany). The predesigned CAD file of the RAI was imported as the reference nominal data, whereas the scanned data were imported as the actual data to be analysed. The alignment process was performed in two steps: in the first step, a pre-alignment was done to align the actual data with the nominal data regardless of the initial positions, and in the second step, an automatic best-fit alignment was performed. This alignment minimises the sum of squared deviations between the actual point cloud and the nominal point cloud (Fig. 2B).

The "Surface comparison on actual" inspection was then performed to compare the deviations between the two data sets across the entire surface. In this inspection, the software compares each actual point to a nominal point, by calculating the direct perpendicular distance between each polygon point on the actual data and the nominal data. Since we focused only on the root-shaped portion of the RAI, the coronal portion was excluded from our inspection. This inspection generates a colour map in which blue indicates the areas measured below the CAD surface (inward deviation) and red indicates areas measured above the CAD surface (outward deviation), whereas green represents areas without deviations. The maximum and minimum deviations have been set to  $+500~\mu m$  and  $-500~\mu m$ , respectively.

For the quantitative assessment of deviations, the entire surface comparison dataset (approximately 45,000 surface data points per model) was exported as an American Standard Code for Information Interchange (ASCII) file with the following parameters: default unit (mm); point cloud coordinates; total deviation. From this dataset, the root mean square (RMS) values representing the absolute deviations

Table 1
Study groups, material properties, and manufacturing technology.

Group	Number	Material	Chemical Composition	Manufacturing Technology	Machine name
Printed Titanium (PT)	10	You Grade 2 (SLM Solutions, Lübeck, Germany)	Ti (grade 2)	SLM 3D printing	SLM 250 HL (SLM Solutions, Lübeck, Germany)
Printed Zirconia (PZ)	10	LithaCon 230 3Y (Lithoz, Vienna, Austria)	ZrO <sub>2</sub> 3 mol % Y <sub>2</sub> O <sub>3</sub>	LCM 3D printing	CeraFab System S65 (Lithoz, Vienna, Austria)
Milled Titanium (MT)	5	Rematitan blank Ti5 (DENTAURUM, Ispringen, Germany)	TiAl6V4 (grade 5)	5-Axis CNC milling	RXD-5 (Röders TEC, Soltau, Germany)
Milled Zirconia (MZ)	5	Zirkon BioStar white opaque (SILADENT, Goslar, Germany)	ZrO <sub>2</sub> / Y <sub>2</sub> O <sub>3</sub> / Al <sub>2</sub> O <sub>3</sub>	5-Axis CNC milling	RXP 500 DSC (Röders TEC, Soltau, Germany)

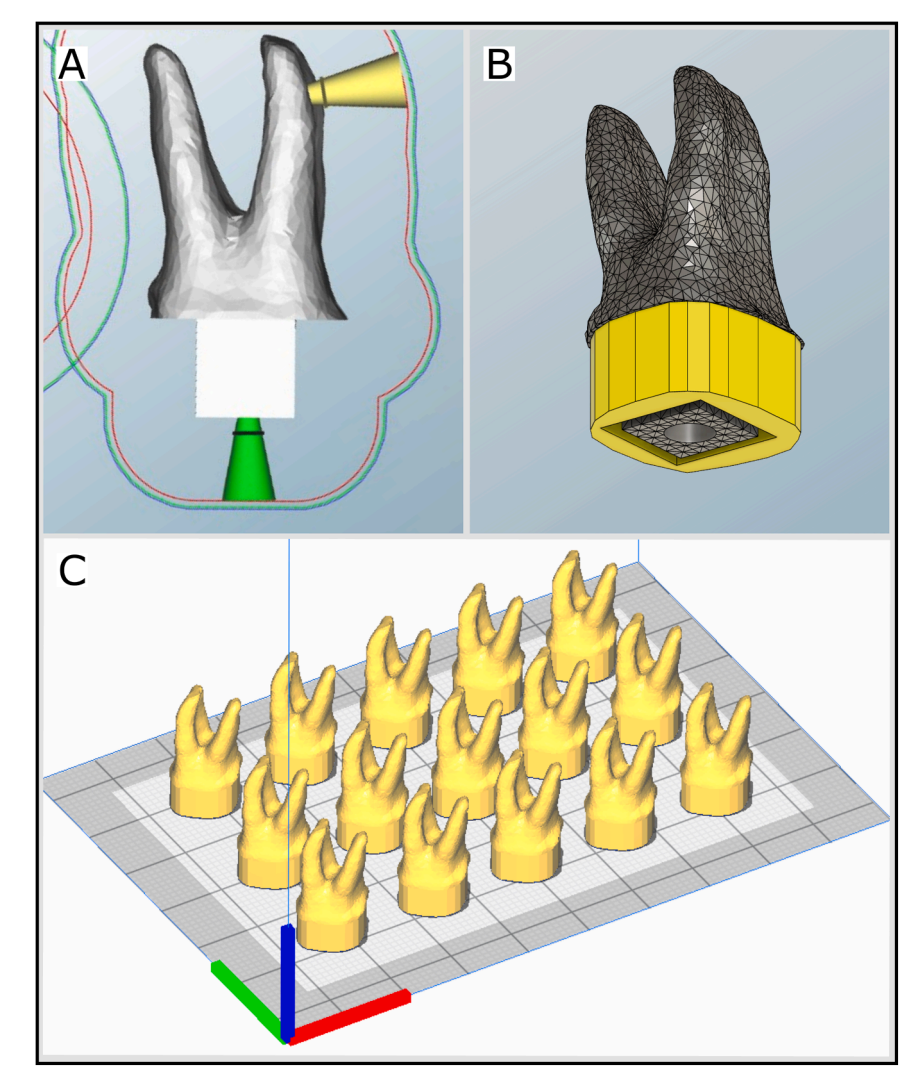


Fig. 1. Preparation of RAI for milling and 3D printing. A. STL file of the RAI with two sprue attachments, ready for milling. B. STL file showing the position of the printing supports of the RAI for 3D printing. C. The alignment and distribution of the RAIs on the 3D printer's bed.

between the nominal and actual data for each superimposition were calculated as follows:

$$RMS = \sqrt{\frac{\sum d^2}{n}}$$

where d is the distance between the actual and nominal data points and n is the number of measurement points.

In addition to the surface comparison, two inspection sections were created for additional in-depth inspection. A "Furcation" section was created at the midpoint of the furcation area by selecting the Y plane as

the reference plane to intersect the RAI buccolingually, and an "Apex" section was created at the junction between the apical third and the middle third of the root portion by selecting the Z plane to intersect the RAI axially (Fig. 2C).

Finally, precision (intragroup comparison) was calculated by cross-comparing different scans in each group (n=45 for the PT and PZ groups and n=10 for the MT and MZ groups), whereas trueness (intergroup comparison) was calculated by comparing the actual scan data in each group to the nominal reference data (n=10 for the PT and PZ groups and n=5 for the MT and MZ groups) as detailed in Fig. 3.

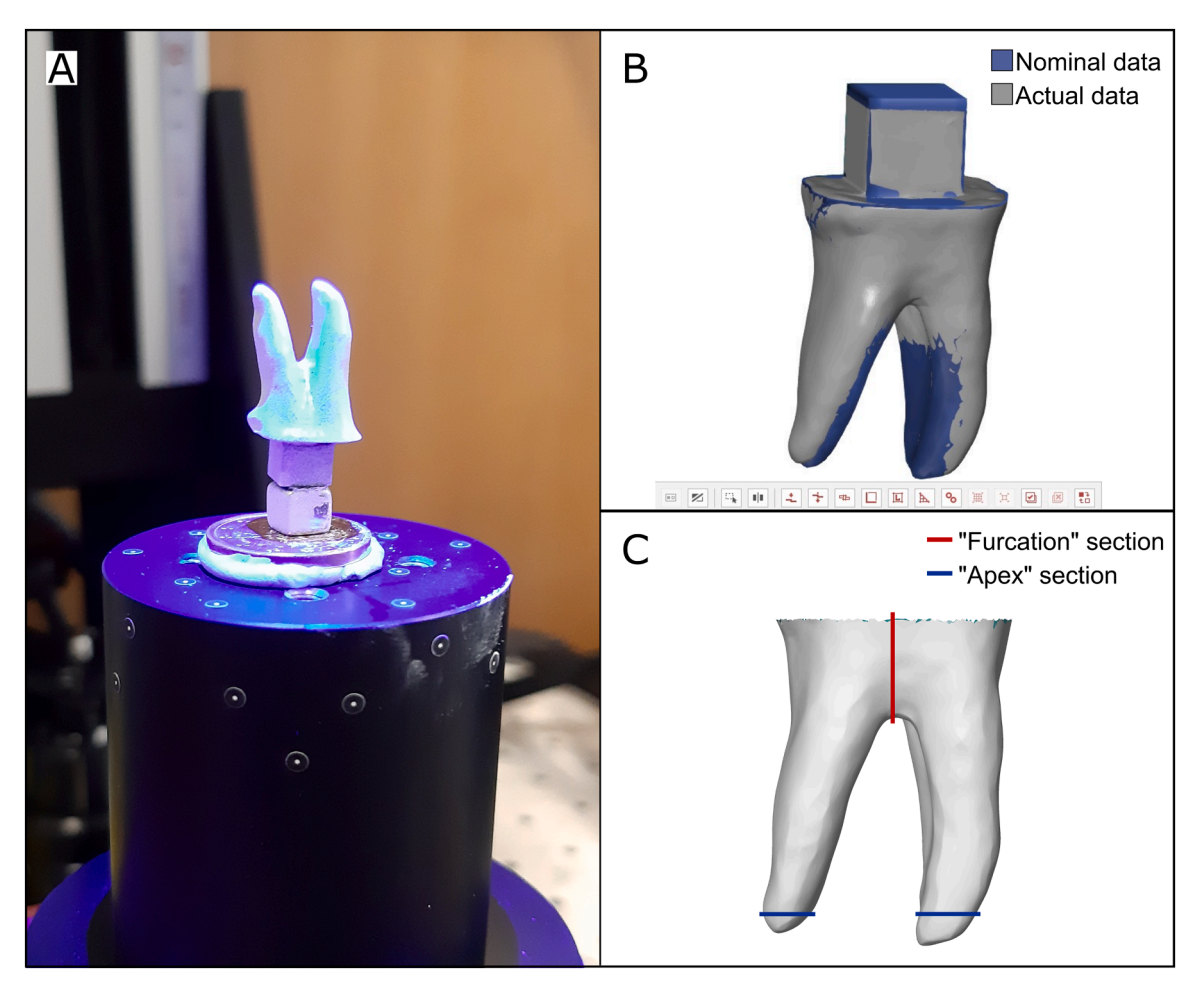


Fig. 2. Preparatory steps for the 3D analysis. A. Optical scanning of the RAI using the Atos Core 80 blue-light scanner (GOM GmbH, Braunschweig, Germany). B. Automatic best-fit alignment of the actual data to the nominal data (GOM Inspect Suite 2020, GOM GmbH, Braunschweig, Germany). C. Schematic representation of the inspection sections with the buccolingual "Furcation" section in the middle of the furcation area and the axial "Apex" section at the junction between the apical third and the middle third of the root portion of the RAI.

#### 2.4. Statistical analysis

The sample size was determined using the freeware (G\*Power 3.1.9.7, Düsseldorf, Germany) based on the results of previously published studies [33,36]. The alpha value and study power (1- $\beta$  err prob) were set to 0.05 and 95%, respectively. Based on our parameters, a minimum total sample size of 20 (5 per group) was required. As the 3D printed samples were more affordable, we were able to increase the number of samples for PT and PZ groups to 10 instead of 5, considering the use of the appropriate statistical tests for unequal sample sizes.

The numerical data are represented as mean and standard deviation (SD) values. Shapiro-Wilk's test was used to test for normality. Homogeneity of variances was tested using Levene's test. The data showed normal distribution and variance homogeneity. One-way ANOVA test followed by Tukey's post hoc test were used for intergroup comparisons. The significance level was set to  $p \leq 0.05$  for all tests, and the statistical analysis was performed with R statistical analysis software version 4.0.4 for Windows  $^1$ .

#### 3. Results

The overall results of precision and trueness are summarised in Table 2. Concerning precision, there was a statistically significant difference in RMS values between the four groups (p<0.001). PZ showed the highest precision with an RMS value of only 21 ( $\pm 5.9$ )  $\mu m$ ; however, no significant difference in precision existed among the other groups. Regarding trueness, there was a significant difference in RMS values between the four groups (p<0.001). MZ exhibited the highest trueness result with an RMS value of 66.4 ( $\pm 2.6$ )  $\mu m$ , whereas MT exhibited the lowest trueness result with an RMS value of 164.3 ( $\pm 22.9$ )  $\mu m$ . Since all samples in each group had similar precision and trueness patterns, a representative image was selected for each group. (Figs. 4 and 5).

It was observed that the maximum deviations are concentrated in the furcation area of MT and the apical area of PZ (Fig. 4), as confirmed also by the inspection sections. The "furcation" inspection section showed that MT had the highest RMS value (612.3  $\mu m$ ), followed by PZ, whereas MZ and PT had the lowest RMS values of 81.7  $\mu m$  and 78.1  $\mu m$ , respectively. For the "apex" section, PZ showed the highest RMS value (197.3  $\mu m$ ), whereas MZ had the lowest RMS value of 45.3  $\mu m$  (Figs. 6 and 7).

When assigning maximum failure thresholds (tolerances) for deviation (100, 200, and 300  $\mu m$ , respectively), MZ presented the lowest percentage of failure, with only 9.9% of the surface exceeding the 100  $\mu m$  tolerance, whereas for both 200  $\mu m$  and 300  $\mu m$  tolerances, PT presented the lowest percentage of failures, with 0.14% and 0.01% of

<sup>&</sup>lt;sup>1</sup> R Core Team (2020). R: A language and environment for statistical computing. R Foundation for Statistical Computing, Vienna, Austria. URL https://www.R-project.org/.

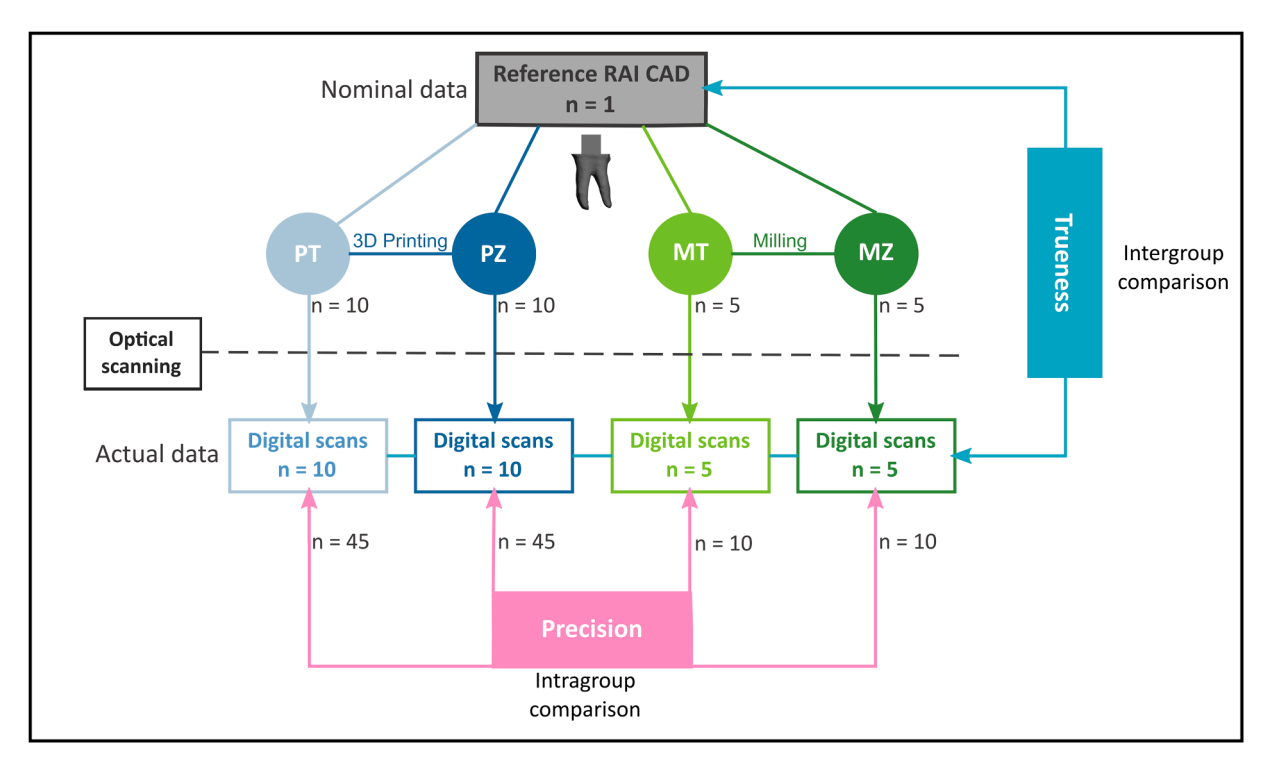


Fig. 3. Flowchart of the study design, starting from the RAI CAD reference file to the group comparison in terms of precision and trueness. RAI, root analogue implant; CAD, computer-aided design.

 Table 2

 Precision, trueness, and inspection section results of the four groups.

		•		0 1	
Group		p value			
	Precision Trueness		Inspectio	n section	
			Furcation	Apex	
PT	$\begin{array}{c} \textbf{32.8} \pm \\ \textbf{7.1}^{\textbf{A}} \end{array}$	$77.9 \pm 4.2^{C}$	$78.1\pm33.2^{C}$	$72.5\pm6.0^B$	<0.001 *
PZ	$\begin{array}{l} 21.0 \; \pm \\ 5.9^{\text{B}} \end{array}$	$99.9\pm7.2^{B}$	$121.4 \pm \\21.5^{\mathrm{B}}$	$197.3 \pm 17.4^{\mathrm{A}}$	<0.001 *
MT	$\begin{array}{c} \textbf{32.2} \pm \\ \textbf{6.8}^{\textbf{A}} \end{array}$	$164.3 \pm 22.9^{\mathrm{A}}$	$612.3 \pm \\63.6^{\mathrm{A}}$	$76.6\pm4.6^B$	<0.001 *
MZ	$\begin{array}{l} 30.0 \; \pm \\ \textbf{4.5}^{A} \end{array}$	$66.4\pm2.6^{D}$	$81.7 \pm 19.7^{BC}$	$45.3\pm2.1^{\mathrm{C}}$	<0.001 *

RMS: root mean square. Different superscript letters indicate a statistically significant difference within the same column.

the surface exceeding the tolerance, respectively, as shown in Table 3 and Figs. 8 and 9. Finally, by comparing the volume of the four groups to the original volume of the RAI CAD model, we observed that MT showed the highest volume change with a volume difference of +7.9% and MZ showed the lowest volume change with a volume difference of +1.0%, while PT was the only group to show a negative volume change of almost -5.0% (Table 3).

#### 4. Discussion

In our study, we evaluated the dimensional accuracy of titanium and zirconia RAIs fabricated by 3D printing and milling. Accuracy was represented by both precision (intra-group comparison) and trueness (inter-group comparison). The four implant groups were optically scanned and superimposed on the reference nominal data using automatic best-fit alignment, and the RMS deviation was used for the 3D analysis. Based on the results of this in vitro study, the null hypothesis that there is no statistical difference in accuracy between the four tested

groups has to be rejected for both precision and trueness.

The evaluation of dimensional accuracy is of crucial importance for the assessment of the primary stability of RAIs [35], which in turn is essential for osseointegration [37]. Unlike conventional TI, which achieves its primary stability by extending the osteotomy 3–5 mm apical to the alveolus during immediate implant placement, RAI obtains its primary stability from the good fit between the implant and the socket, which forms a good congruence with the extraction site [38]. Therefore, any mismatch with the alveolus will result in a reduced contact between the bone and the implant, which will decrease the primary stability and lead to implant failure [35].

Aiming to mimic the clinical workflow of RAI placement, we have designed the RAI based on the natural root form of tooth 47 using CBCT data acquisition and CAD software [39]. Our decision to use a multi-rooted tooth was primarily based on our interest in evaluating accuracy in the critical furcation area, which to our knowledge has not been investigated in previous studies. Furthermore, incongruence in this critical area also has a detrimental effect on RAI insertion [35].

The RMS value reflects the degree of deviation of the scanned data. A low RMS value represents well-matched data overlap, which means higher values for trueness and precision [40]. According to Rossini et al. [41] and Sohmura et al. [42], a clinically acceptable error of 200 to 300  $\mu m$  is acceptable for diagnostic casts. However, other studies suggest a higher accuracy in fixed and implant prosthodontics, with clinically acceptable error ranging from 50 to 150  $\mu m$  [24,28]. In the present study, the mean deviations ranged from 21.0 to 32.8  $\mu m$  for precision assessment and from 66.4 to 164.3  $\mu m$  for trueness assessment.

The results of this in vitro study reveal that the precision of 3D printed zirconia is statistically higher than that of the other groups. Precision can be defined here as the degree of repeatability of measured samples of the same group [32]. PZ showed higher precision result compared to the milled groups. Such result supports the findings of Marcel et al. [22] who compared milled and 3D printed bite splints in terms of accuracy. In their study, they concluded that the precision of 3D printed bite splints surpasses that of milled bite splints. A similar conclusion was reached by Schönherr et al. [28] who reported high

<sup>\*</sup> Significant (*p*≤0.05)

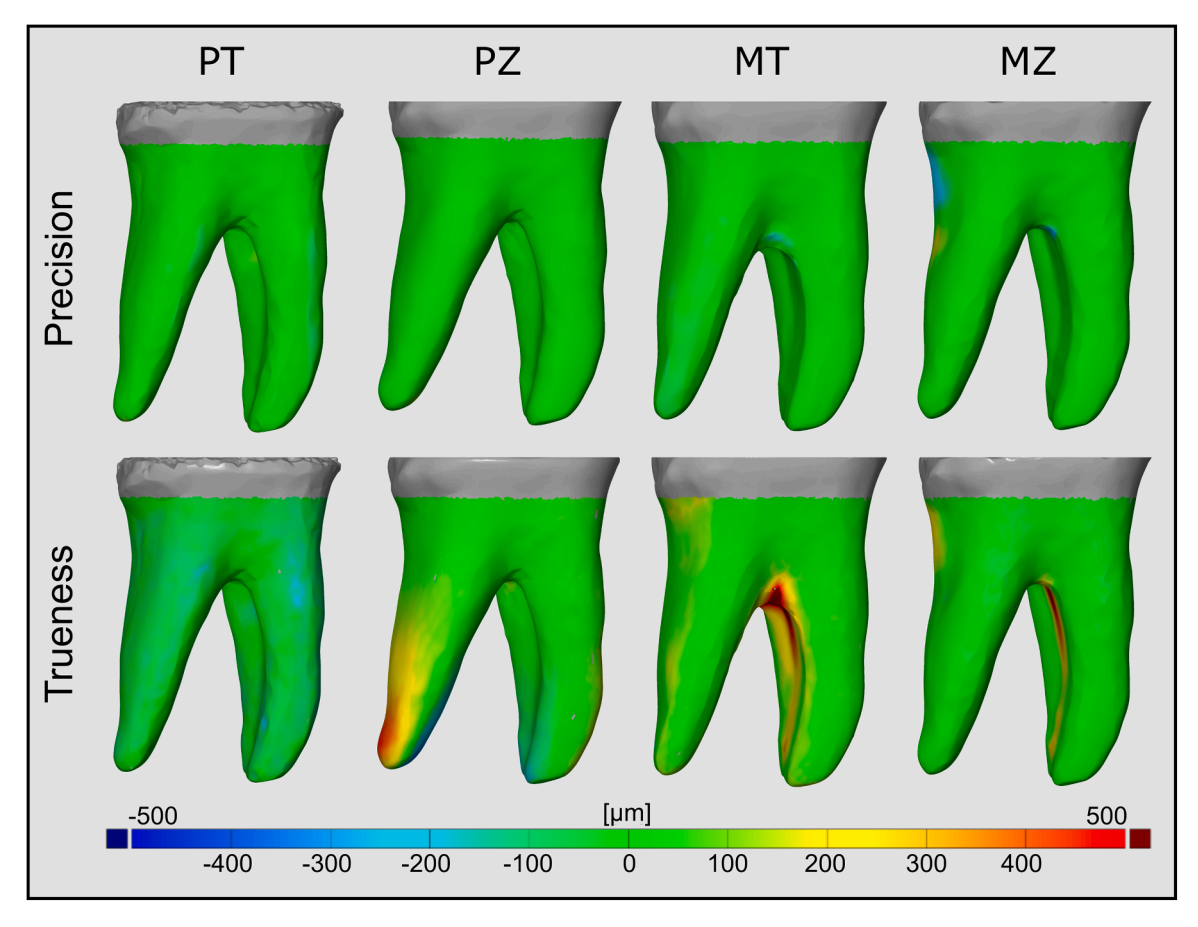


Fig. 4. Colour map showing precision and trueness 3D analysis. The outward deviation is indicated by red colour whereas the inward deviation is indicated by blue colour. The maximum and minimum deviations have been set to  $+500 \mu m$  and  $-500 \mu m$ , respectively. (For interpretation of the references to color in this figure legend, the reader is referred to the web version of this article.).

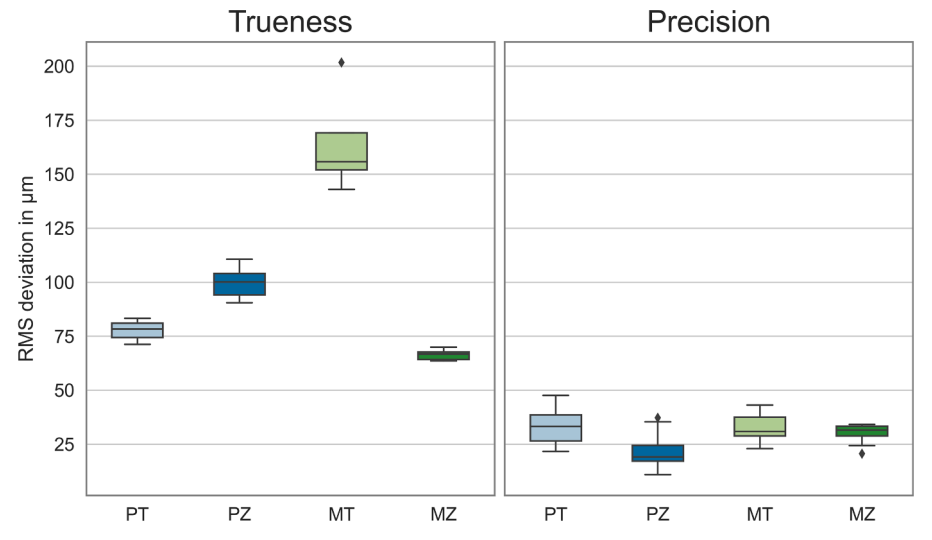
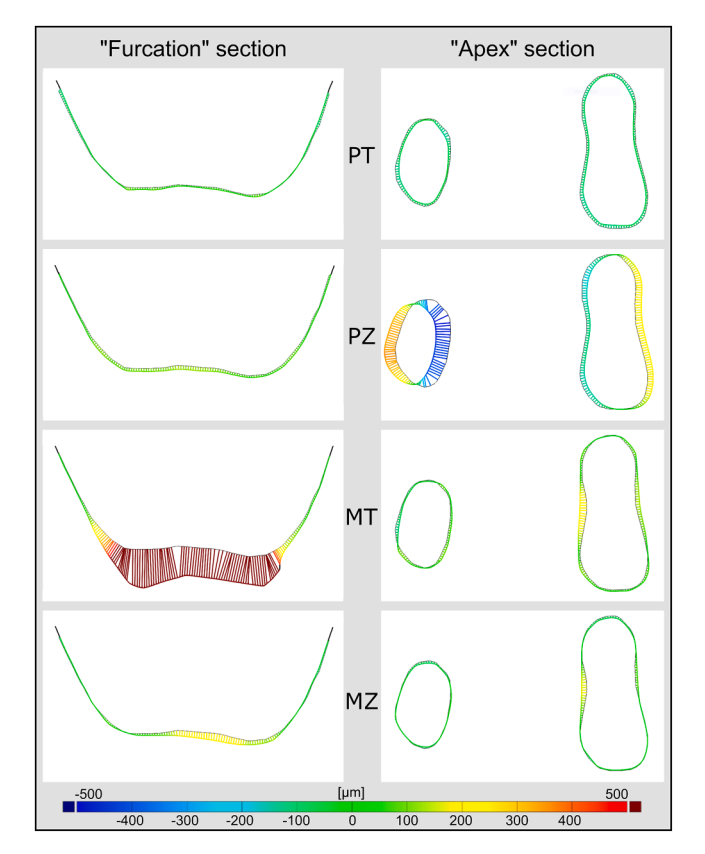


Fig. 5. Boxplot graphs showing the trueness and precision values using root mean square (RMS) deviation.

reproducibility of crowns processed with LCM.

Our results in terms of trueness showed that milled zirconia had the highest trueness among the four test groups with respect to the reference CAD file. Specifically, MZ showed significantly higher trueness compared to PZ. A similar conclusion was reached in a recent in vitro study by Lerner et al. [21] who compared the accuracy of milled and 3D printed monolithic zirconia crowns (MZCs). Similar to our study, the

authors used the CerafabS65 LCM based printer for the fabrication of the 3D printed crowns and a 5-axis machine for the fabrication of the milled crowns. To evaluate trueness, they used the (90-10)/2 method, the absolute average (ABS AVG) method, and the RMS method, which is also used in our study. The authors reported that milled MZCs had higher trueness than 3D printed MZCs, and both groups showed high precision that is compatible with the clinical use.



**Fig. 6.** Colour map showing "Furcation" and "Apex" inspection sections. The outward deviation is indicated by red colour whereas the inward deviation is indicated by blue colour. The maximum and minimum deviations have been set to  $+500~\mu m$  and  $-500~\mu m$ , respectively. (For interpretation of the references to color in this figure legend, the reader is referred to the web version of this article.).

The main reason for the decreased trueness in PZ is the relatively high deviation in the apical region (about 197  $\mu$ m). In LCM technology, the zirconia green body shrinks during the subsequent debinding and sintering process. Thus, the manufacturer recommends a shrinkage compensation of 1.354 during production [43]. However, warpage during the sintering process is another problem [28]. Since the RAI is placed upside down on the build platform, the maximum warpage is observed in the least supported apical region. The problem with this

warpage is that it could interfere with the proper insertion of the RAI due to incongruence with the socket. Yet, this deformation could be reduced by providing support in this area, as suggested in the study by Schönherr et al. [28].

The evaluation of the trueness of titanium-made RAIs revealed that 3D-printed RAIs using SLM technology had a significantly higher trueness value than the milled RAIs, which had the lowest trueness among the four groups (RMS value of around 164 µm for MT), the high trueness of RAIs printed with SLM technology is consistent with several studies [11,30,31]. Chen et al. [11] evaluated the biomechanical performance of RAIs fabricated by SLM by measuring the dimensional accuracy along with other properties such as the surface roughness and the tensile strength. They concluded that RAIs produced by SLM technology showed high strength and adequate dimensional accuracy. In another in vitro study, Ciocca et al. [44] evaluated the accuracy of metal frameworks for full-arch dental restorations on implants by comparing a new hybrid technique (SLM printing/milling) with the conventional milling technique. They concluded that the accuracy of metal frameworks fabricated with the novel hybrid technique was significantly higher than that of the conventional technique.

While AM proved suitable for the fabrication of titanium RAIs, SM showed poor results in terms of trueness. This is directly related to the manufacturing process; in AM, the object is formed by layer-by-layer deposition, while in SM, the object is milled with cutting burs that cut into a preformed block. In this process, the CAM software calculates the needed milling paths and recognises where critical undercuts are located. The geometry of the milled object is thus limited by the size and

**Table 3**Change in volume with respect to the reference nominal data and percentage of failure at different tolerances.

Group	Volume difference (%), Mean $\pm$ SD	-	Fail percentage (%), Mean $\pm$ SD Tolerance ( $\mu$ m)			
		100	200	300		
PT	$-5.0\pm0.5^{\mathrm{D}}$	$19.0 \pm 4.3^{B}$	$\begin{array}{c} 0.1 \pm \\ 0.3^{C} \end{array}$	$\begin{array}{c} 0.01 \pm \\ 0.03^{C} \end{array}$	<0.001 *	
PZ	$+4.5\pm0.6^{B}$	$\begin{array}{c} 28.2 \; \pm \\ 2.5^A \end{array}$	$\begin{array}{c} \textbf{5.7}  \pm \\ \textbf{1.7}^{\textbf{A}} \end{array}$	$\begin{array}{c} 1.32 \pm \\ 0.67^{\mathrm{B}} \end{array}$	<0.001 *	
MT	$+7.9\pm0.5^{A}$	$17.9 \pm 2.4^{B}$	$\begin{array}{l} 6.9 \; \pm \\ 0.4^A \end{array}$	$\begin{array}{c} 3.94 \pm \\ 0.11^{A} \end{array}$	<0.001 *	
MZ	$+1.0\pm0.4^{\rm C}$	$\begin{array}{l} 9.9 \pm \\ 1.3^{\text{C}} \end{array}$	$\begin{array}{c} 2.6 \; \pm \\ 0.3^B \end{array}$	$\begin{array}{c} \textbf{1.20} \pm \\ \textbf{0.07}^{\text{B}} \end{array}$	<0.001 *	

Different superscript letters indicate a statistically significant difference within the same column.

<sup>\*</sup> Significant (p≤0.05)

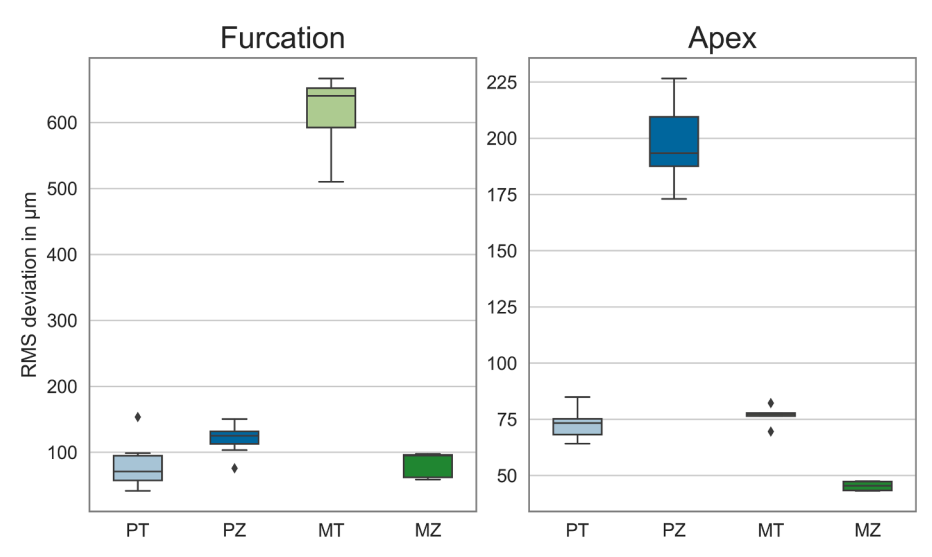


Fig. 7. Boxplot diagrams showing the values of the "Furcation" and "Apex" inspection sections using root mean square (RMS) deviation.

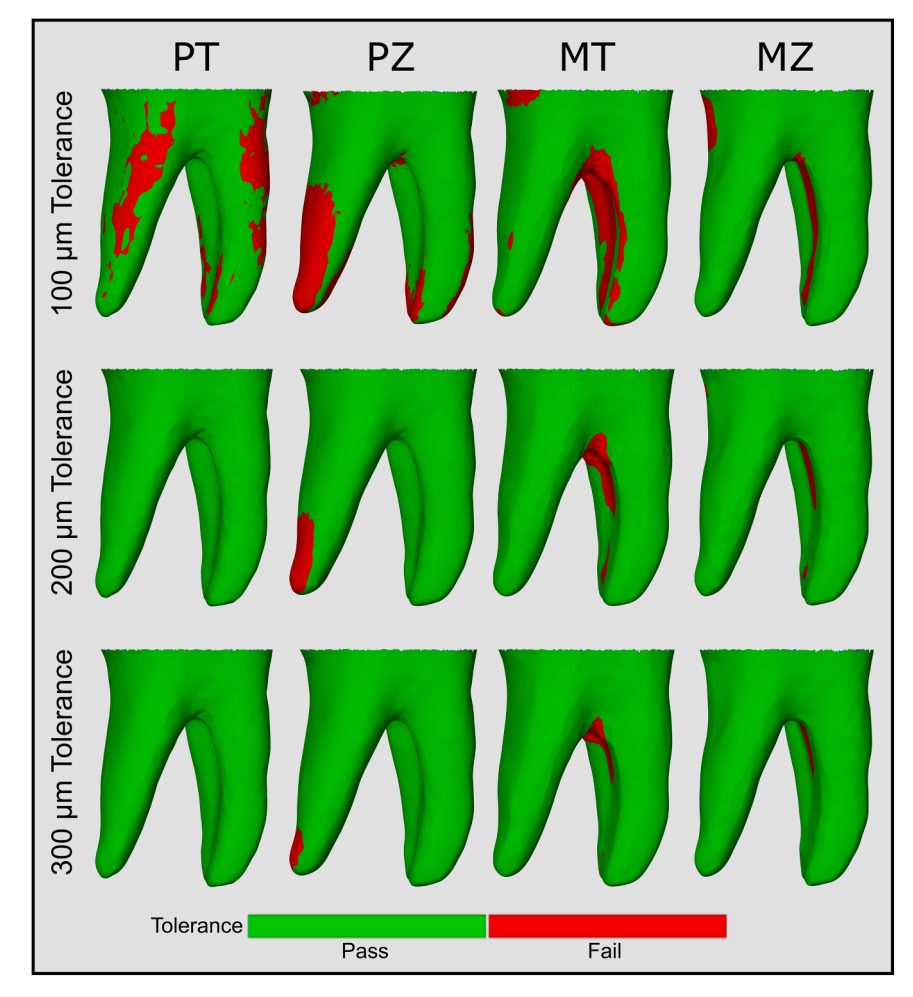


Fig. 8. Colour map showing the percentage of failure when assigning 100  $\mu m$ , 200  $\mu m$ , and 300  $\mu m$  tolerance values. (For interpretation of the references to color in this figure legend, the reader is referred to the web version of this article.).

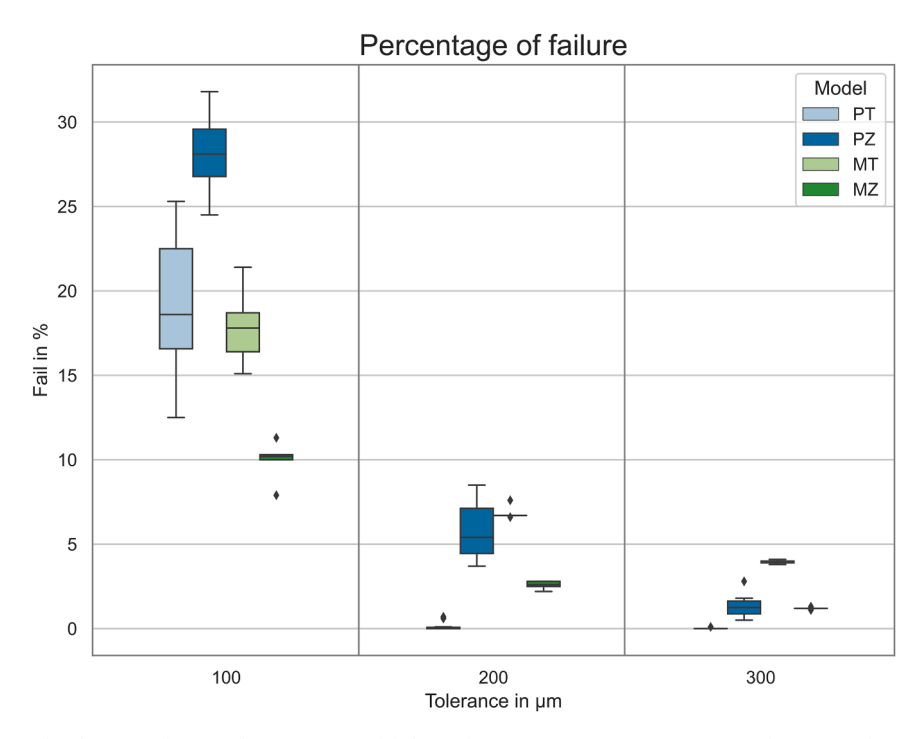


Fig. 9. Boxplot diagrams showing the percentage of failure when assigning 100  $\mu m$ , 200  $\mu m$ , and 300  $\mu m$  tolerance values.

the milling path of the cutting bur, which means that in deep concave surfaces, the diameter of the bur should be smaller than the diameter to be milled. Otherwise, the milled surface will be over-contoured in this area [22]. This is clearly visible in the furcation area of the milled titanium RAI.

Noteworthy, in contrast to milled titanium, milled zirconia exhibited less deviation in the furcation area even though it was milled with a 5-axis CNC machine with the same setup and tool size. This could be due to the fact that zirconia is milled with an oversize of 20–25% to compensate for sintering shrinkage according to the enlargement factor recommended by the manufacturer [45]. This creates more space for the milling paths and allows the cutting burs to reach areas that cannot be reached during the true-size milling, as is the case with milled titanium RAIs.

Another finding that can be clearly observed, especially from the inspection sections in Fig. 6, is that AM could reproduce the surface anatomy of the RAIs more precisely than SM with better reproduction of concave areas and undercuts. This finding is consistent with previous studies [19,22,26], but contradicts the claims of Lerner et al. [21] that AM cannot accurately reproduce deep and narrow grooves on the occlusal surface. Our explanation for this contradiction is that the printing supports in Lerner's study were placed on the occlusal surface, where it is difficult for the technician to remove the supports without under- or over-polishing the surface, whereas in the present study, the printing supports were placed on the coronal portion of the RAI, so they do not impair the accuracy results, which are confined to the root-shaped section of the RAI.

By taking advantage of 3D superimposition analysis, we can be confident that our results are reliable and not biased because the superimposition and 3D analyses were performed digitally via computer, which is superior to traditional manual measurements. In addition, we have included the entire dataset of surface points to fully measure all deviations in the three spatial directions, which is more reliable than the traditional linear assessment method by selecting finite measuring points, which may introduce operator bias, especially in irregular anatomical geometries such as the RAI [23,33].

A potential limitation of this study is that it is an *in vitro* study with a limited sample size, where the implications of the observed deviations on implant placement and primary stability were not evaluated. In addition, the results are valid only for the materials and machines used in our study. Further studies with additional manufacturing protocols are therefore required for a thorough evaluation of the accuracy of the RAIs.

At the end of our study, we speculate to the best of our knowledge that this is the first study to comprehensively discuss the dimensional accuracy of titanium and zirconia RAIs manufactured by both the additive and subtractive methods. The promising results in terms of precision and trueness encourage a broader implementation of 3D printed and milled RAIs in immediate implant cases. However, the inherent volumetric changes of the different materials during fabrication should be considered, possibly by adjusting the shrinkage compensation factor or the CAD file. This shrinkage occurs mainly during melting of the titanium powder in SLM printing and during the heat treatment phase of the 3D printed and milled zirconia. Finally, we recommend confining the use of milled titanium to single-rooted RAI cases only.

#### 5. Conclusions

Within the limitations of this study (*in vitro*, limited sample size, limited manufacturing protocols), both the manufacturing process and material selection had a significant impact on RAI accuracy. The 3D printed zirconia RAIs exhibited the highest precision, whereas the milled zirconia RAIs exhibited the highest trueness, followed by the 3D printed titanium RAIs. Within this study, both the 3D printed and milled RAIs showed clinically acceptable accuracy levels, excluding milled titanium RAIs, which showed high deviation in the furcation region. Finally,

additive manufacturing showed better reproduction of deep concave surfaces and less accessible areas compared to subtractive manufacturing.

#### **Authors Contributions**

M. Aldesoki: Conceptualization, Methodology, Software, Formal analysis, Data curation, Writing- Original draft preparation, Visualization. L. Keilig: Investigation, Data curation, Writing- Reviewing and Editing, Supervision. I. Dörsam: Methodology, Validation, Writing-Reviewing and Editing. B. Evers-Dietze: Methodology and Software. TM Elshazly: Software, Data curation, Visualization. C. Bourauel: Methodology, Validation, Writing- Reviewing and Editing, Supervision.

All authors have read and agreed to the published version of the manuscript.

#### **Funding**

This work was supported by a grant from the German academic exchange service (DAAD, 2019/20, 57440921).

#### **Declaration of interests**

The authors declare that they have no known competing financial interests or personal relationships that could have appeared to influence the work reported in this paper.

#### Acknowledgements

The authors are grateful to Fachhochschule Nordwestschweiz for providing the 3D printed titanium implants.

#### References

- [1] V. Moraschini, L.A.D.C. Poubel, V.F. Ferreira, E.D.S.P. Barboza, Evaluation of survival and success rates of dental implants reported in longitudinal studies with a follow-up period of at least 10 years: a systematic review, Int. J. Oral Maxillofac. Surg. 44 (2015) 377–388, https://doi.org/10.1016/j.ijom.2014.10.023.
- [2] M. Figliuzzi, F. Mangano, C. Mangano, A novel root analogue dental implant using CT scan and CAD/CAM: selective laser melting technology, Int. J. Oral Maxillofac. Surg. 41 (2012) 858–862, https://doi.org/10.1016/j.ijom.2012.01.014.
- [3] R.U. Koh, I. Rudek, H.L. Wang, Immediate implant placement: positives and negatives, Implant Dent. 19 (2010) 98–108, https://doi.org/10.1097/ ID.0B013E3181D47EAF.
- [4] J.R. Beagle, The immediate placement of endosseous dental implants in fresh extraction sites, Dent. Clin. North Am. 50 (2006) 375–389, https://doi.org/ 10.1016/j.cden.2006.03.003.
- [5] K.M. Regish, D. Sharma, D.R. Prithviraj, An overview of immediate root analogue zirconia implants, J. Oral Implantol. 39 (2013), https://doi.org/10.1563/AAID-JOI-D-10-00208
- [6] R. Saeidi Pour, C. Freitas Rafael, M.L.P.D. Engler, D. Edelhoff, G. Klaus, O. Prandtner, M. Berthold, A. Liebermann, Historical development of root analogue implants: a review of published papers, Br. J. Oral Maxillofac. Surg. 57 (2019) 496–504, https://doi.org/10.1016/j.bjoms.2019.01.021.
- [7] L.T. Yong, Single stage immediate implant placements in the esthetic zone, J. Oral Implantol. 38 (2012), https://doi.org/10.1563/AAID-JOI-D-11-00152.
- [8] W.A. Ghuneim, In situ tooth replica custom implant: A 3-dimensional finite element stress and strain analysis, J. Oral Implantol. 39 (2013), https://doi.org/ 10.1563/AAID-JOI-D-10-00142.
- [9] D. Moin, B. Hassan, D. Wismeijer, Immediate nonsubmerged custom root analog implants: a prospective pilot clinical study, Int. J. Oral Maxillofac. Implants 33 (2018) e37–e44. https://doi.org/10.11607/jomi.6048.
- [10] D. Anssari Moin, B. Hassan, D. Wismeijer, A novel approach for custom three-dimensional printing of a zirconia root analogue implant by digital light processing, Clin. Oral Implants Res. 28 (2017) 668–670, https://doi.org/10.1111/clr.12859.
- [11] J. Chen, Z. Zhang, X. Chen, C. Zhang, G. Zhang, Z. Xu, Design and manufacture of customized dental implants by using reverse engineering and selective laser melting technology, J. Prosthet. Dent. 112 (2014), https://doi.org/10.1016/j. prosdent.2014.04.026, 1088-1095.E1.
- [12] F.G. Mangano, M. De Franco, A. Caprioglio, A. MacChi, A. Piattelli, C. Mangano, Immediate, non-submerged, root-analogue direct laser metal sintering (DLMS) implants: a 1-year prospective study on 15 patients, Lasers Med. Sci. 29 (2014) 1321–1328, https://doi.org/10.1007/s10103-013-1299-0.
- [13] T. Dantas, S. Madeira, M. Gasik, P. Vaz, F. Silva, Customized root-analogue implants: a review on outcomes from clinical trials and case reports, Materials (Basel) 14 (2021) 1–14, https://doi.org/10.3390/ma14092296.

- [14] F. Beuer, J. Schweiger, D. Edelhoff, Digital dentistry: an overview of recent developments for CAD/CAM generated restorations, Br. Dent. J. 204 (2008), https://doi.org/10.1038/sj.bdj.2008.350.
- [15] M. Kanazawa, M. Inokoshi, S. Minakuchi, N. Ohbayashi, Trial of a CAD/CAM system for fabricating complete dentures, Dent. Mater. J. 30 (2011), https://doi. org/10.4012/dmj.2010-112.
- [16] G. Bosch, A. Ender, A. Mehl, A 3-dimensional accuracy analysis of chairside CAD/ CAM milling processes, J. Prosthet. Dent. 112 (2014) 1425–1431, https://doi.org/ 10.1016/j.prosdent.2014.05.012.
- [17] M. Zeltner, I. Sailer, S. Mühlemann, M. Özcan, C.H.F. Hämmerle, G.I. Benic, Randomized controlled within-subject evaluation of digital and conventional workflows for the fabrication of lithium disilicate single crowns. Part III: marginal and internal fit, J. Prosthet. Dent. 117 (2017) 354–362, https://doi.org/10.1016/j. prosdent.2016.04.028.
- [18] K. Son, B.Y. Yu, T.H. Yoon, K.B. Lee, Comparative study of the trueness of the inner surface of crowns fabricated from three types of lithium disilicate blocks, Appl. Sci. 9 (2019), https://doi.org/10.3390/app9091798.
- [19] H.T. Yau, T.J. Yang, Y.K. Lin, Comparison of 3-D printing and 5-axis milling for the production of dental e-models from intra-oral scanning, Comput. Aided Des. Appl. 13 (2016) 32–38, https://doi.org/10.1080/16864360.2015.1059186.
- [20] Y.G. Jeong, W.S. Lee, K.B. Lee, Accuracy evaluation of dental models manufactured by CAD/CAM milling method and 3D printing method, J. Adv. Prosthodont. 10 (2018) 245–251, https://doi.org/10.4047/jap.2018.10.3.245.
- [21] H. Lerner, K. Nagy, N. Pranno, F. Zarone, O. Admakin, F. Mangano, Trueness and precision of 3D-printed versus milled monolithic zirconia crowns: an in vitro study, J. Dent. 113 (2021), 103792, https://doi.org/10.1016/j.jdent.2021.103792.
- [22] R. Marcel, H. Reinhard, K. Andreas, Accuracy of CAD/CAM-fabricated bite splints: milling vs 3D printing, Clin. Oral Investig. 24 (2020) 4607–4615, https://doi.org/ 10.1007/s00784-020-03329-x.
- [23] Z. chen Zhang, P. lun Li, F. ting Chu, G. Shen, Influence of the three-dimensional printing technique and printing layer thickness on model accuracy, J. Orofac. Orthop. 80 (2019) 194–204, https://doi.org/10.1007/s00056-019-00180-y.
- [24] Y. Etemad-Shahidi, O.B. Qallandar, J. Evenden, F. Alifui-Segbaya, K.E. Ahmed, Accuracy of 3-dimensionally printed full-arch dental models: a systematic review, J. Clin. Med. 9 (2020) 1–18, https://doi.org/10.3390/jcm9103357.
- [25] M. Revilla-León, M. Özcan, Additive manufacturing technologies used for processing polymers: current status and potential application in prosthetic dentistry, J. Prosthodont. 28 (2019) 146–158, https://doi.org/10.1111/ jour.12801
- [26] J. Schweiger, D. Edelhoff, J.F. Güth, 3d printing in digital prosthetic dentistry: an overview of recent developments in additive manufacturing, J. Clin. Med. 10 (2021), https://doi.org/10.3390/jcm10092010.
- [27] M.L. Griffith, J.W. Halloran, Freeform fabrication of ceramics via stereolithography, J. Am. Ceram. Soc. 79 (1996) 2601–2608, https://doi.org/ 10.1111/j.1151-2916.1996.tb09022.x.
- [28] J.A. Schönherr, S. Baumgartner, M. Hartmann, J. Stampfl, Stereolithographic additive manufacturing of high precision glass ceramic parts, Materials (Basel) 13 (2020) 5–7, https://doi.org/10.3390/ma13071492.
- [29] Y. Uçar, İ. Aysan Meriç, O. Ekren, Layered manufacturing of dental ceramics: fracture mechanics, microstructure, and elemental composition of lithographysintered ceramic, J. Prosthodont. 28 (2019) e310–e318, https://doi.org/10.1111/ jopr.12748.
- [30] D.A. Moin, B. Hassan, P. Mercelis, D. Wismeijer, Designing a novel dental root analogue implant using cone beam computed tomography and CAD/CAM

- technology, Clin. Oral Implants Res. 24 (2013) 25–27, https://doi.org/10.1111/j.1600-0501.2011.02359.x.
- [31] M. Revilla-León, M. Sadeghpour, M. Özcan, A review of the applications of additive manufacturing technologies used to fabricate metals in implant dentistry, J. Prosthodont. 29 (2020) 579–593, https://doi.org/10.1111/jopr.13212.
- [32] ISO-5725-1, Accuracy (Trueness and Precision) of Measurement Methods and Results. Part 1: General Principles and Definitions, ISO, Geneva, 1994 n.d.
- [33] S.-J. Jin, I.-D. Jeong, J.-H. Kim, W.-C. Kim, Accuracy (trueness and precision) of dental models fabricated using additive manufacturing methods, Int. J. Comput. Dent. 21 (2018) 107–113. http://www.ncbi.nlm.nih.gov/pubmed/29967903.
- [34] O. Rungrojwittayakul, J.Y. Kan, K. Shiozaki, R.S. Swamidass, B.J. Goodacre, C. J. Goodacre, J.L. Lozada, Accuracy of 3D printed models created by two technologies of printers with different designs of model base, J. Prosthodont. 29 (2020) 124–128, https://doi.org/10.1111/jopr.13107.
- [35] D.A. Moin, B. Hassan, A. Parsa, P. Mercelis, D. Wismeijer, Accuracy of preemptively constructed, Cone Beam CT-, and CAD/CAM technology-based, individual Root Analogue Implant technique: an in vitro pilot investigation, Clin. Oral Implants Res. 25 (2014) 598–602, https://doi.org/10.1111/clr.12104.
- [36] N. Kalberer, A. Mehl, M. Schimmel, F. Müller, M. Srinivasan, CAD-CAM milled versus rapidly prototyped (3D-printed) complete dentures: an in vitro evaluation of trueness, J. Prosthet. Dent. 121 (2019) 637–643, https://doi.org/10.1016/j. prosdent.2018.09.001.
- [37] N. Lioubavina-Hack, N.P. Lang, T. Karring, Significance of primary stability for osseointegration of dental implants, Clin. Oral Implants Res. 17 (2006), https:// doi.org/10.1111/j.1600-0501.2005.01201.x.
- [38] W. Pirker, D. Wiedemann, A. Lidauer, A.A. Kocher, Immediate, single stage, truly anatomic zirconia implant in lower molar replacement: a case report with 2.5 years follow-up, Int. J. Oral Maxillofac. Surg. 40 (2011), https://doi.org/10.1016/j. ijom/2010.08.003
- [39] B. Westover, Three-dimensional custom-root replicate tooth dental implants, Oral Maxillofac. Surg. Clin. North Am. 31 (2019) 489–496, https://doi.org/10.1016/j. coms.2019.03.010.
- [40] G.H. Park, K.B. Da Son, K.B. Lee, Feasibility of using an intraoral scanner for a complete-arch digital scan, J. Prosthet. Dent. 121 (2019) 803–810, https://doi. org/10.1016/J.PROSDENT.2018.07.014.
- [41] G. Rossini, S. Parrini, T. Castroflorio, A. Deregibus, C.L. Debernardi, Diagnostic accuracy and measurement sensitivity of digital models for orthodontic purposes: a systematic review, Am. J. Orthod. Dentofac. Orthop. 149 (2016), https://doi.org/ 10.1016/j.ajodo.2015.06.029.
- [42] Y.H. Sohmura, H. Satoh, J. Takahashi, K. Takada, Complete 3-d reconstruction of dental cast shape using perceptual grouping, IEEE Trans. Med. Imaging 20 (2001), https://doi.org/10.1109/42.959306.
- [43] L. Conti, D. Bienenstein, M. Borlaf, T. Graule, Effects of the layer height and exposure energy on the lateral resolution of zirconia parts printed by lithographybased additive manufacturing, Materials (Basel) 13 (2020), https://doi.org/ 10.3390/mal3061317.
- [44] L. Ciocca, R. Meneghello, G. Savio, L. Scheda, C. Monaco, M.R. Gatto, C. Micarelli, P. Baldissara, Manufacturing of metal frameworks for full-arch dental restoration on implants: a comparison between milling and a novel hybrid technology, J. Prosthodont. 28 (2019) 556–563, https://doi.org/10.1111/JOPR.13067.
- [45] E. Kontonasaki, P. Giasimakopoulos, A.E. Rigos, Strength and aging resistance of monolithic zirconia: an update to current knowledge, Jpn. Dent. Sci. Rev. 56 (2020) 1–23, https://doi.org/10.1016/j.jdsr.2019.09.002.

## 3.2 Study 2

Evaluation of micromotion in multirooted root analogue implants embedded in synthetic bone blocks: an in vitro study

Mostafa Aldesoki, Christoph Bourauel, Tarek M. Elshazly, Erik Schkommodau, Ludger Keilig

BMC Oral Health (2024)

https://doi.org/10.1186/s12903-024-03854-1

Impact factor: 2.6

RESEARCH Open Access

# Evaluation of micromotion in multirooted root analogue implants embedded in synthetic bone blocks: an in vitro study

Mostafa Aldesoki<sup>1\*</sup>, Christoph Bourauel<sup>1</sup>, Tarek M. Elshazly<sup>1</sup>, Erik Schkommodau<sup>2</sup> and Ludger Keilig<sup>1,3</sup>

#### **Abstract**

**Background** While conventional threaded implants (TI) have proven to be effective for replacing missing teeth, they have certain limitations in terms of diameter, length, and emergence profile when compared to customised root analogue implants (RAI). To further investigate the potential benefits of RAIs, the aim of this study was to experimentally evaluate the micromotion of RAIs compared to TIs.

**Methods** A 3D model of tooth 47 (mandibular right second molar) was segmented from an existing cone beam computed tomography (CBCT), and a RAI was designed based on this model. Four RAI subgroups were fabricated as follows: 3D-printed titanium (PT), 3D-printed zirconia (PZ), milled titanium (MT), milled zirconia (MZ), each with a sample size of n=5. Additionally, two TI subgroups (B11 and C11) were used as control, each with a sample size of n=5. All samples were embedded in polyurethane foam artificial bone blocks and subjected to load application using a self-developed biomechanical Hexapod Measurement System. Micromotion was quantified by analysing the load/displacement curves.

**Results** There were no statistically significant differences in displacement in Z-axis (the loading direction) between the RAI group and the TI group. However, within the RAI subgroups, PZ exhibited significantly higher displacement values compared to the other subgroups (p < 0.05). In terms of the overall total displacement, the RAI group showed a statistically significant higher displacement than the TI group, with mean displacement values of 96.5  $\mu$ m and 55.8  $\mu$ m for the RAI and TI groups, respectively.

**Conclusions** The RAI demonstrated promising biomechanical behaviour, with micromotion values falling within the physiological limits. However, their performance is less predictable due to varying anatomical designs.

Keywords Dental implants, Stability, Patient specific, Biomechanics, Motion, 3D printing, Milling, Titanium, Zirconia

\*Correspondence: Mostafa Aldesoki

mostafadesoki86@gmail.com; aldesoki@uni-bonn.de

<sup>1</sup> Dental School, Oral Technology, University Hospital Bonn, Welschnonnenstr.17, 53111 Bonn, Germany

#### **Background**

The average survival rate of dental implants after ten years of clinical use is almost 95%, establishing them the best treatment choice for replacing missing and severely decayed teeth [1]. The International Team for Implantology (ITI) consensus conference has classified dental implants based on the insertion protocol as follows: a) immediate implant placement on the day of tooth extraction, b) early implant placement with soft tissue healing typically occurring after 4 to 8 weeks, c) early implant



© The Author(s) 2024. **Open Access** This article is licensed under a Creative Commons Attribution 4.0 International License, which permits use, sharing, adaptation, distribution and reproduction in any medium or format, as long as you give appropriate credit to the original author(s) and the source, provide a link to the Creative Commons licence, and indicate if changes were made. The images or other third party material in this article are included in the article's Creative Commons licence, unless indicated otherwise in a credit line to the material. If material is not included in the article's Creative Commons licence and your intended use is not permitted by statutory regulation or exceeds the permitted use, you will need to obtain permission directly from the copyright holder. To view a copy of this licence, visit http://creativecommons.org/licenses/by/4.0/. The Creative Commons Public Domain Dedication waiver (http://creativecommons.org/publicdomain/zero/1.0/) applies to the data made available in this article, unless otherwise stated in a credit line to the data.

<sup>&</sup>lt;sup>2</sup> Institute for Medical Engineering and Medical Informatics, University of Applied Sciences and Arts Northwestern Switzerland, Muttenz, Switzerland

<sup>&</sup>lt;sup>3</sup> Department of Prosthodontics, Dental School, University Hospital Bonn, Bonn, Germany

Aldesoki et al. BMC Oral Health (2024) 24:99 Page 2 of 9

placement with partial bone healing taking place approximately 12 to 16 weeks later, and d) late implant placement after complete bone healing after of least 6 months [2].

Immediate implant placement has many advantages, including shortening the overall treatment time, reducing costs, and decreasing the number of surgical interventions [3]. Additionally, it helps preserving the height and width of the alveolar bone while minimising marginal bone loss following extraction [3–5]. However, the decreased primary stability due to the incongruence between the implant and the alveolus, as well as the difficult implant placement can be a real surgical challenge [6–8].

One of the treatment alternatives to conventional threaded implants (TIs) is the use of fully customised root-analogue implants (RAIs) [9]. The concept of RAI was initially introduced by Hodosh et al. in 1969 as a heat-processed methyl methacrylate implant. However, it was deemed unsuccessful after failure to achieve osseointegration [10]. In 1992, the technique was reintroduced using pure titanium instead of polymer, leading to successful osseointegration [7].

Such RAIs are the product of the combined technologies of computer-aided design/computer-aided manufacturing (CAD/CAM) and cone beam computed tomography (CBCT) [6, 11]. The idea of the RAI is to replace a tooth scheduled for extraction through an immediate implant placement by designing the RAI with similar dimensions to the original root anatomy based on CBCT. Thus, a perfect congruence between the implant and the empty socket could be achieved, unlike TI [12]. The expected benefits include a reduced number of surgeries, simple and straightforward placement, improved primary stability and immediate soft tissue support [13–15].

RAIs are produced using either subtractive or additive manufacturing techniques [16]. Subtractive manufacturing employs a milling process facilitated by computer numerical control (CNC) milling machines. These machines are categorized based on the number of axes they operate on, ranging from 3-axis to 5-axis machines [17, 18]. On the other hand, additive manufacturing involves 3D printing, a method that transforms a digital model into a physical object by depositing materials layer by layer [19, 20].

A notable advancement in additive manufacturing is the use of lithography-based ceramic manufacturing (LCM) for 3D printing advanced ceramics. In this process, a ceramic slurry coated with a photosensitive resin is hardened layer by layer using a light-emitting diode device [21]. Another significant technique in additive manufacturing is selective laser melting (SLM), which involves fusing powdered metal using a high-power fibre laser in an inert environment. The laser precisely melts each layer onto the preceding one, creating a solid object through the accumulation of thousands of micro-welds [22, 23].

The stability of the implant in the alveolar bone is of crucial importance for successful osseointegration [24]. The term micromotion in dental implants refers to the subtle displacement of an implant in relation to the surrounding tissue, which cannot be observed with the naked eye [25]. Studies have suggested that for successful osseointegration, the micromotion between the implant and bone should not exceed a threshold value of 150 µm [26, 27]. Implant stability can be classified into primary and secondary stability. Primary stability is achieved by the mechanical retention of the implant during initial insertion, whereas secondary stability is reached after consecutive bone remodelling processes and complete healing. Consequently, primary stability is considered a mechanical phenomenon, while secondary stability is a biological phenomenon influenced by osseointegration [28]. Many factors influence the primary stability of the implant, such as the quality and quantity of the surrounding bone and the implant geometry; changing the implant-bone contact area by increasing the length or width of the implant could enhance the primary stability [9, 29].

The biomechanical behaviour of dental implants has been extensively investigated in various studies [26, 30, 31]. However, there is a notable gap in research regarding the specific biomechanical behaviour of RAIs. Hence, the aim of this study was to experimentally evaluate the micromotion of multi-rooted titanium and zirconia RAIs by analysing their load/displacement curves. The null hypothesis stated that there would be no statistically significant difference in micromotion among the examined groups or subgroups (p > 0.05).

#### **Methods**

#### Study design

Two implant designs were used in this study: a custom-designed RAI and a traditional TI as a control. The RAI was designed based on a CBCT scan of a dentate mandible using the following scanning parameters: beam accelerating voltage of 90 kV, X-ray current of 12 mA, voxel dimension of 75  $\mu$ m, and total scanning time of 15 s. The total number of slices was 668. The CBCT scan was processed using a 3D medical image processing software (Mimics 22; Materialise, Leuven, Belgium) and the right mandibular second molar (tooth 47) was segmented based on histogram analysis. The segmented tooth was subsequently imported into a 3D modelling software (3-matic 15; Materialise, Leuven, Belgium), to finalise the

Aldesoki et al. BMC Oral Health (2024) 24:99 Page 3 of 9

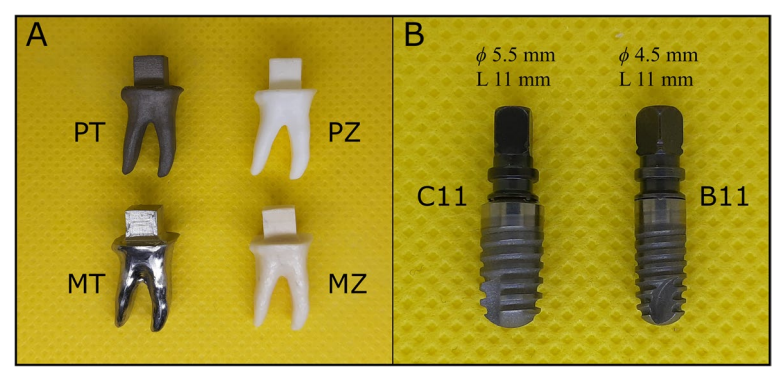


Fig. 1 Overview of the examined implant groups. A Root analogue implant (RAI) group, including PT, PZ, MT, and MZ subgroups. B Threaded Implant (TI) group, comprising C11 and B11 subgroups. Φ, Diameter; L, Length

design of the RAI based on the anatomy of the tooth. The coronal portion was designed as an idealised cube with a side length of 5 mm to facilitate further biomechanical investigations.

The RAIs were produced using two methods: milling and 3D printing, with both titanium and zirconia as materials of choice. Milling was performed with 5-axis CNC milling machines, whereas LCM and SLM technologies were used for the 3D printing of zirconia and titanium RAIs, respectively. During 3D printing, the printing supports were placed on the overhanging coronal surface around the idealised cube, and the layer thickness was set to 25  $\mu$ m. A total of 20 RAIs were fabricated and categorized into four subgroups (n=5) based on the manufacturing method: 3D printed titanium (PT), 3D printed zirconia (PZ), milled titanium (MT), and milled zirconia (MZ).

As a control group, conventional TI were included (Ankylos; Dentsply-Friadent, Mannheim, Germany). The TI group was divided into two subgroups (n=5) based on implant size: B11 subgroup with a diameter of 4.5 mm and length of 11 mm, and C11 subgroup with a diameter of 5.5 mm and length of 11 mm (Fig. 1).

#### Biomechanical analysis

For the biomechanical testing, the implants were inserted into test blocks made of polyurethane foam artificial bone (Sawbones; Pacific Research Laboratories, Vashon, USA). These test blocks were comprised of two layers: a 2 mm-thick layer of epoxy filled with short glass fibres (type #3401–01, density 1.64 g/cm³), which simulated cortical bone, and a 40 mm-thick layer of rigid polyure-thane foam (type #1522–01, density 0.16 g/cm³), which simulated cancellous bone. The TIs were screwed into Sawbones following the surgical protocol provided by the manufacturer (Fig. 2A). As for the RAIs, a socket-shaped cavity, resembling the negative replica of the root-shaped

RAI, was initially drilled in the Sawbones (Fig. 2B). Prior to insertion into the Sawbones, the surface of the RAIs was coated with a thin layer of resin (PalaXpress; Heraeus Kulzer GmbH, Wasserburg, Germany) to secure a tight attachment between the RAI and the Sawbones. Each specimen was then firmly fastened to the base of the specimen holder using PalaXpress resin (Fig. 2C).

The samples were inserted into a custom-developed biomechanical Hexapod Measurement System (HexMeS) [32]. HexMeS is specifically designed to apply various forces on small objects like dental implants. It consists of three main components: a high-precision hexapod robot (PI M-850.50; Physik Instrumente, Karlsruhe, Germany) capable of precise translations and rotations with a resolution of less than 1 µm and 5 µrad. Additionally, the system incorporates a high-precision 3D force/torque sensor (ATI FTSGamma 130/10; SCHUNK GmbH & Co. KG, Lauffen/Neckar, Germany) for force and torque measurements, as well as an optical system for precise position detection, consisting of an aluminium cube with three pinholes, each 2 µm in diameter (Melles-Griot, Bensheim, Germany) illuminated by a laser beam (35) mW, 658 nm; Laser 2000, Wessling, Germany), and three video cameras with macro zoom optics (JAI CV-M1; Stemmer-Imaging, Puchheim, Germany). This setup enables the accurate tracking of micromotions in the specimens under load application by monitoring the pinholes through the video cameras (Fig. 3).

The samples were mounted on the HexMeS with the implant aligned parallel to the Z-axis. The laser-illuminated aluminium cube was securely attached to the top of the samples, and a spoon-shaped lever arm was connected to the implant. This configuration allowed any movement of the Hexapod to be transmitted as a force to the implant (Fig. 4).

The samples were indirectly loaded by programming the Hexapod to perform a loading cycle of 1.5 mm

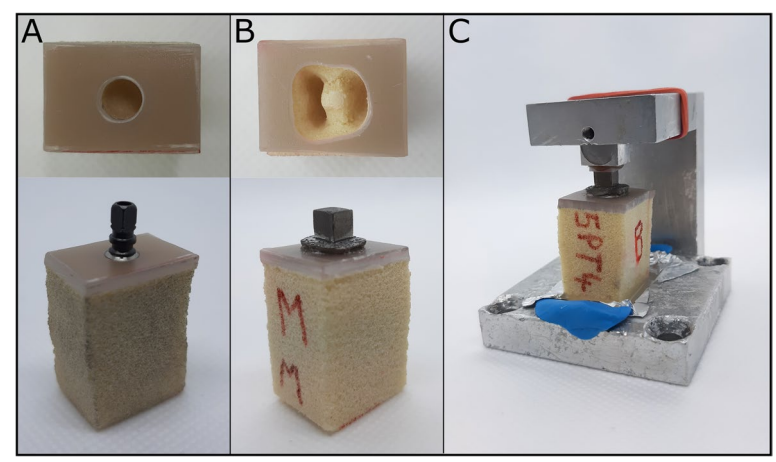


**Fig. 2** Preparation of specimens for biomechanical testing. **A** Preparation of the osteotomy of the polyurethane foam block to insert the TI. **B** Preparation of the osteotomy of the polyurethane foam block to insert the RAI. **C** Secure fixation of the specimen to the specimen holder using resin. The metal structure on top of the specimen holder holds the aluminium cube in place during preparation, and is removed before measuring the specimen

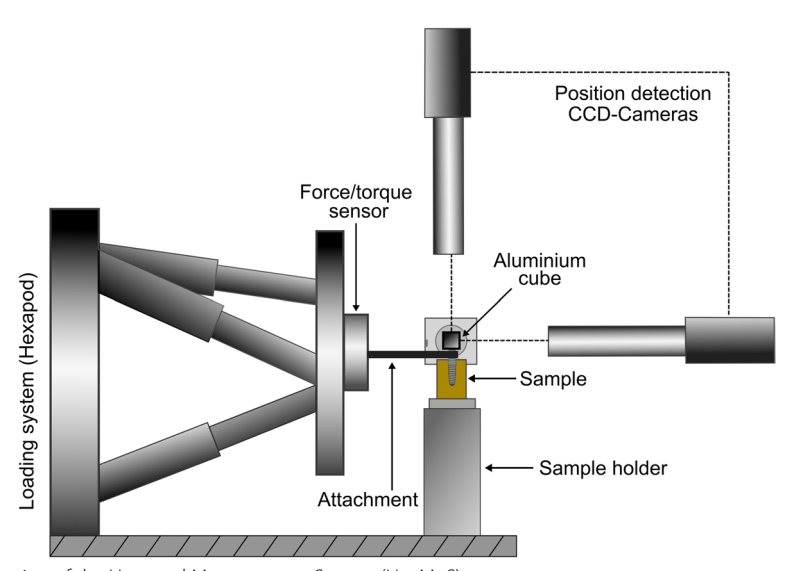


Fig. 3 Schematic representation of the Hexapod Measurement System (HexMeS)

translation in the negative Z direction, followed by a release cycle in the positive Z direction until reaching the zero position (150 steps of 0.02 mm each). The applied force and torque were recorded by the force/torque system, and simultaneously the displacement of the implant (translation and rotation) was recorded by tracking the laser-illuminated pinholes through the video cameras. The collected data were exported in CSV format (comma separated values) for further data analysis.

#### Statistical analysis

The numerical data are represented as mean values and standard deviations. The normality of the data was

assessed using Shapiro–Wilk's test, while Levene's test was employed to test for homogeneity of variances. The data showed a parametric distribution, homogeneity of variances, and were analysed using nested ANOVA. Estimated marginal means were compared using t-test with p-value adjustment using Tukey's method. A significance level of  $p \le 0.05$  was chosen for all statistical tests. The statistical analysis was performed using R statistical analysis software, version 4.1.3 for Windows  $^1$ .

<sup>&</sup>lt;sup>1</sup> R Core Team (2022). R: A language and environment for statistical computing. R Foundation for Statistical Computing, Vienna, Austria. URL https://www.R-project.org/

Aldesoki et al. BMC Oral Health (2024) 24:99 Page 5 of 9

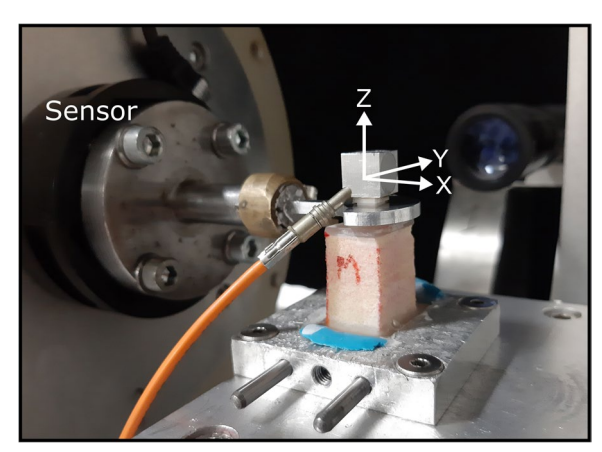


**Fig. 4** Experimental setup for biomechanical testing. The specimen was securely mounted on the HexMeS system with the implant aligned parallel to the Z axis. An aluminium cube, illuminated by a laser, was attached to the specimen. A loading cycle of 1.5 mm translation in the negative Z direction was applied, followed by a releasing cycle. The resultant force and torque were accurately recorded by the force/torque sensor

total displacement. The mean values and the standard deviation for all measured displacements in loading direction at a force of 50 N are shown in Table 1.

The nested ANOVA model for displacement (Z) revealed that there was no statistically significant difference between the two parent groups. The mean displacement for the TI group was 44  $\mu$ m compared to 48  $\mu$ m for the RAI group. However, a significant interaction within the nested subgroup variable (p=0.002) was observed. Notably, among the RAI subgroups, PZ exhibited the highest displacement value of 71  $\mu$ m, while the differences in displacement between the PT, MT, and MZ subgroups were statistically insignificant (Fig. 6 and Tables 1 and 2).

Comparisons of estimated marginal means presented in Table 3 and Fig. 7 indicated that there were no statistically significant differences among the parent groups (p=0.325) or the two subgroups within the TI group (p=0.964). However, within the RAI group, PZ had significantly higher values than the other subgroups (p<0.05).

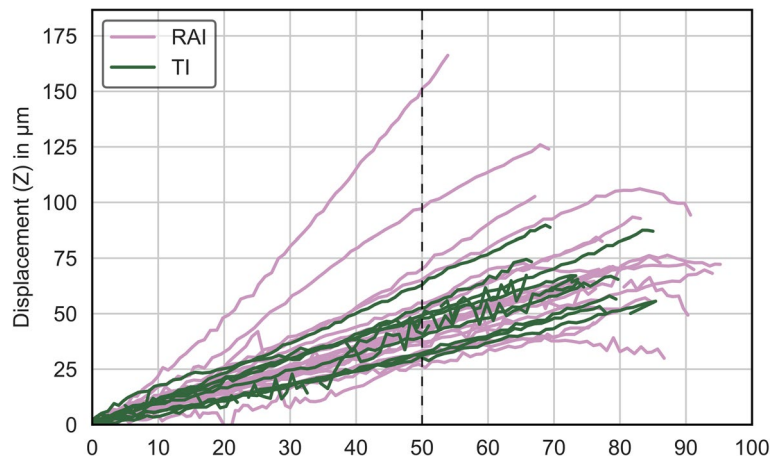


Fig. 5 Line chart showing load/displacement curves for all specimens. The dashed line represents the maximum force (50 N) chosen to include all the specimens

#### Results

The maximum magnitude of forces recorded by the force sensor ranged from 64 to 96 N, whereas the produced maximum displacements ranged from 40  $\mu$ m to 178  $\mu$ m. Owing to the different magnitudes of forces, a maximum force of 50 N was chosen for the different specimens to include all specimens (Fig. 5).

The HexMeS allows for the precise measurement of micromovements in each sample, by tracking both the translations and rotations in the three spatial directions. Particular attention will be given to the displacement in the loading direction (Z-axis), as well as the

**Table 1** Displacement (Z) and total displacement values for both groups and subgroups

Group	Displace Mean ± S	ment in µm D	Subgroup	Displacement in μm Mean ± SD		
	(Z)	Total		(Z)	Total	
TI	44 ± 11	56±17	B11	43±8	57±13	
			C11	$44 \pm 14$	$55 \pm 22$	
RAI	$48 \pm 18$	$96 \pm 49$	PT	$39 \pm 10$	$61 \pm 7$	
			PZ	$71 \pm 22$	125 ± 59	
			MT	$43\pm0$	112±55	
			MZ	$40 \pm 8$	$88 \pm 44$	

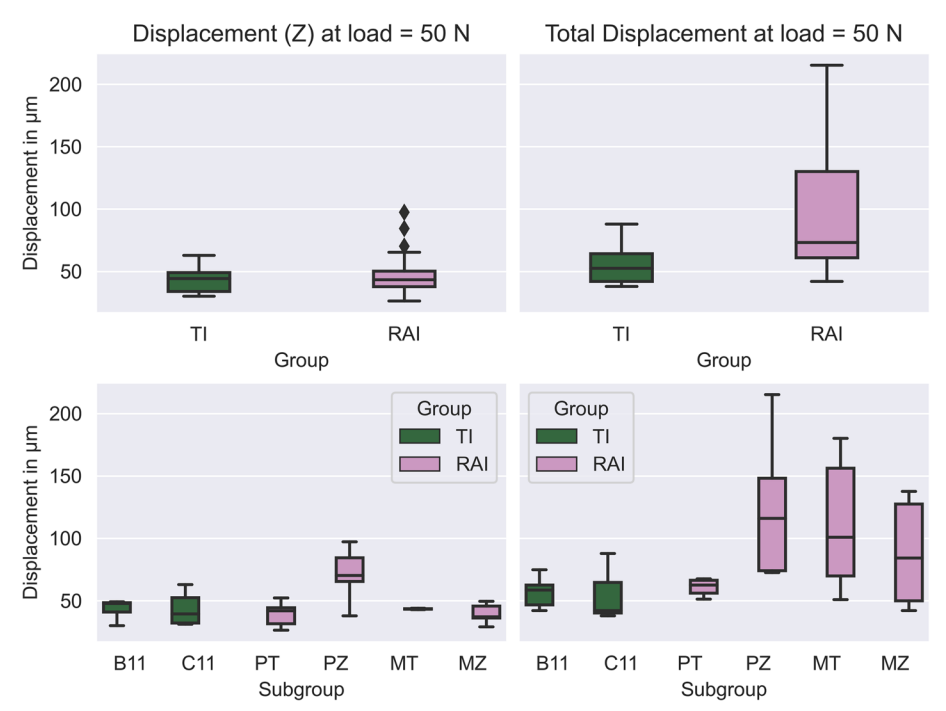


Fig. 6 Boxplot diagrams illustrating displacement (Z) and total displacement values across groups and subgroups

**Table 2** Nested ANOVA model for displacement (Z) and total displacement

Parameter	Displacement (Z)					Total Displacement				
	SS	DF	MS	F	P	SS	DF	MS	F	р
Group	155.61	1	155.61	1.01	0.325	11,046.31	1	11,046.31	7.23	0.013*
Subgroup	3487.78	4	871.94	5.65	0.002*	11,995.26	4	2998.81	1.96	0.133
Error	3703.53	24	154.31			36,664.18	24	1527.67		

SS Sum of squares, DF Degrees of freedom, MS Mean squares, FF value, pP value

**Table 3** Comparison of estimated marginal mean for displacement (Z)

Comparisons	Estimate	95% CI		Statistic	p value
		Lower	Upper		
TI—RAI	-4.83	-14.80	5.10	-1.00	0.325
B11 – C11	-0.35	-16.57	15.86	-0.04	0.964
PT—PZ	-31.75	-53.42	-10.08	-4.04	0.003*
PT—MT	-4.12	-25.8	17.55	-0.53	0.952
PT—MZ	-0.33	-22.01	21.34	-0.04	1.00
PZ—MT	27.63	5.95	49.3	3.52	0.009*
PZ—MZ	31.42	9.75	53.09	4.00	0.003*
MT-MZ	3.79	-17.88	25.46	0.48	0.962

<sup>\*</sup>Significant (p < 0.05)

Regarding total displacement, the nested ANOVA model showed that the RAI group had a statistically significantly higher displacement compared to the TI group (p=0.013), with mean displacement values of 96  $\mu$ m and 56  $\mu$ m for the RAI and TI groups, respectively. However, the effect of the nested subgroup variable was not statistically significant (p=0.133) (Fig. 6 and Tables 1 and 2).

#### Discussion

The objective of this study was to compare the biomechanical behaviour of multi-rooted RAIs and TIs. In vitro load/displacement curves were analysed to assess the micromotion of both implant designs. Based on the study findings, the null hypothesis, which implies no

<sup>\*</sup> Significant (p < 0.05)

Aldesoki et al. BMC Oral Health (2024) 24:99 Page 7 of 9

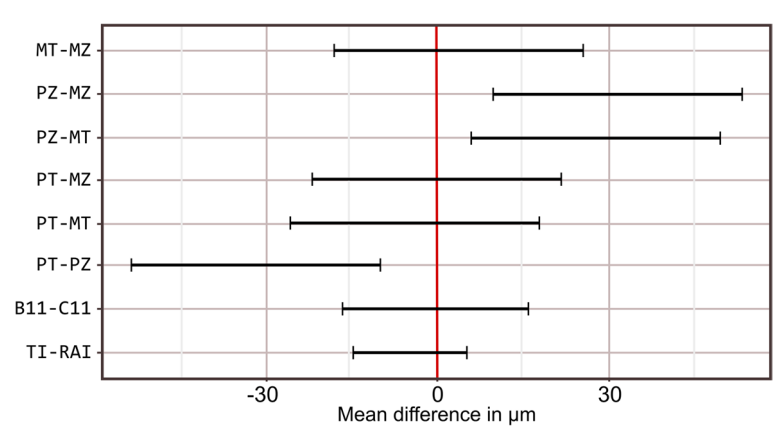


Fig. 7 Interval plot showing the variation in estimated marginal means for displacement along the Z-axis

statistically significant difference in micromotion among the examined groups or subgroups, was partially rejected.

One of the determining key factors for successful implant placement is implant stability, whether it is assessed immediately after implant placement or after osseointegration. The stability of dental implants has been evaluated in literature by various methods including Periotest<sup>®</sup> and resonance frequency analysis [29]. In the present in vitro study, we have used micromotion as an indicator of implant stability by comparing the produced displacements of TI and RAI under specific loading conditions [31, 33].

Our objective was to replicate the clinical process of placing RAI by utilizing CBCT data acquisition and CAD software to design the RAI according to the natural root shape of tooth 47 [34]. We have specifically chosen a multirooted tooth to explore the intricate mechanical characteristics of such teeth, which have not been thoroughly examined in prior research. The two most common materials used in the manufacturing of RAIs are titanium alloy and zirconia [16, 35]. Owing to the biocompatibility and the remarkable mechanical and physical properties of titanium, it has been widely used for dental implants [36]. Nonetheless, the increasing emphasis on aesthetics has led to the emergence of zirconia as a viable alternative [37]. Zirconia exhibits high biocompatibility, superior flexural strength, reduced bacterial affinity, and the advantage of adjustable white colour [36]. In our study, both titanium alloy and zirconia were selected as materials for the RAIs, using both additive and subtractive manufacturing methods.

Sawbones artificial bone blocks were used instead of cadaver bone to take advantage of their uniform and standardised physical properties. This reduced variability and eliminated the special handling requirements associated with cadaver bone. PalaXpress resin was chosen

to fix the RAIs in the Sawbones, owing to its appropriate working time, stability, and radiopacity, as previously reported in the literature [31]. In contrast, the TIs were firmly inserted into the drilled Sawbones without requiring any resin application.

The results of this study revealed that there was no statistically significant difference in displacements along the loading direction (Z-axis) between the RAIs and the TIs, suggesting comparable stability between the two implant types. These findings are consistent with a study by Gattinger et al. [38], where they compared by finite element analysis the micromotion of RAI and standard implant and reported that the RAI was as good as the standard threaded implant in terms of micromotion. A similar conclusion was reached out by Chen et al. [39] who studied the biomechanical performance of RAI for both the immediate and the delayed loading protocols. They observed increased micromotion in the RAI during immediate loading, but reduced micromotion during the osseointegrated phase with bonded contact simulation, indicating reliable long-term stability.

Based on the findings of a previous study conducted by Aldesoki et al. [34], it was observed that the manufacturing method had a slight impact on the dimensions of the produced RAIs. Taking this into consideration, our study incorporated four RAI subgroups that comprised different combinations of manufacturing techniques and materials. The analysis of estimated marginal means revealed a statistically significant higher displacement in the PZ subgroup compared to the other RAI subgroups (p > 0.5). This observation aligns with the aforementioned study, which reported noticeable warpage at the apical part of the RAI during the manufacturing process specifically in the PZ group [34]. Such warpage may contribute to increased susceptibility of the RAI to displacement or movement under loading conditions.

Aldesoki et al. BMC Oral Health (2024) 24:99 Page 8 of 9

Regarding total displacement, the RAI group exhibited a statistically significant increase in displacement compared to the TI group (p < 0.05). Specifically, the RAI demonstrated increased micromotion along the X and Y axes, while the TI group primarily experienced micromotion along the loading Z axis. This eccentric micromotion behaviour of the RAI can be attributed to its anatomical shape, characterised by asymmetric mesial and distal roots in terms of form and length. Additionally, the experimental loading conditions of the HexMeS setup, where the specimens are indirectly loaded through the spoon-shaped attachment, indirectly contribute to this behaviour. From a biomechanical perspective, the spoon-shaped attachment acts as a lever arm, generating torque on the implant and resulting in rotation around the Y axis, thereby increasing displacement along the X axis.

Noteworthy, the mean micromotion values observed in the RAI were approximately 48  $\mu m$  for displacement along the Z-axis and approximately 96  $\mu m$  for total displacement. These values remain below the maximum threshold value of micromotion crucial for successful osseointegration, which is estimated to be around 150  $\mu m$  [26, 27]. These findings indicate that the range of micromotion exhibited by the RAI is unlikely to impede the osseointegration process.

We presume that this study has effectively investigated the stability of RAI by closely adhering to the clinical workflow and utilizing the latest technologies in RAI preparation. Nevertheless, certain limitations should be considered. Firstly, this is an in vitro study, thus the histological examination of osseointegration was not feasible. Secondly, the fixation of RAI in the artificial bone involved the use of a thin resin layer, which was a crucial step owing to the anatomical shape of RAI and the non-drilling surgical protocol. Finally, the loading of the HexMeS setup could not be done directly on the specimens, and the spoon-shaped load applicator might have introduced an additional torque.

In view of the results of the present study, RAIs showed biomechanical behaviour in terms of stability and micromotion comparable to that of TIs. Moreover, based on previous studies [14, 34], RAIs fabricated by milling or 3D printing showed promising results in terms of dimensional accuracy. Collectively, these findings propose that RAI could serve as a feasible alternative to TI, particularly in immediate implant cases, provided a well-prepared preoperative treatment plan and access to a capable CBCT device. However, it's crucial to note that the tooth to be replaced should lack sharp undercuts that might impede the insertion of the RAI or compromise its proper fit. Nevertheless, further clinical trials and studies are necessary to validate its clinical application.

#### **Conclusions**

After acknowledging the limitations of this study, we drew the following conclusions:

- 1. The RAI exhibited promising biomechanical behaviour, as indicated by micromotion values within physiological limits.
- 2. The stability of the RAI could be influenced by the manufacturing technique.
- 3. Compared to the TI, the biomechanical behaviour of the RAI is less predictable due to its irregular anatomical design.
- 4. Precise definition of the implant geometry is essential to ensure a precise fit and a seamless insertion.

#### **Abbreviations**

TI Threaded implant RAI Root analogue implant

CBCT Cone beam computed tomography ITI International team for implantology

CAD/CAM Computer-aided design/Computer-aided manufacturing

CNC Computer numerical control

LCM Lithography-based ceramic manufacturing

SLM Selective laser melting
HexMeS Hexapod measurement system
CSV Comma separated values

#### Acknowledgements

The authors gratefully acknowledge Dr. Bassam A. Abulnoor for his contribution to the statistical analysis of this research.

#### Authors' contributions

MA: Conceptualization, Methodology, Software, Formal analysis, Data curation, Writing, Original draft preparation, Visualisation. CB: Project administration, Validation, Writing, Reviewing and Editing, Supervision. TME: Investigation, Data curation, Writing, Reviewing and Editing. ES: 3D printing, Reviewing and Editing, Visualisation. LK: Methodology, Investigation, Data curation, Software, Writing, Reviewing and Editing, Supervision. All authors have read and agreed to the published version of the manuscript.

#### **Funding**

Open Access funding enabled and organized by Projekt DEAL. This work was supported by a grant from the German academic exchange service (DAAD, 2019/20, 57440921).

#### Availability of data and materials

The datasets used and/or analysed during the current study available from the corresponding author on reasonable request.

#### **Declarations**

#### Ethics approval and consent to participate

Not applicable.

#### Consent for publication

Not applicable.

#### **Competing interests**

The authors declare no competing interests.

Received: 18 September 2023 Accepted: 3 January 2024 Published online: 17 January 2024

#### References

- Moraschini V, Poubel LADC, Ferreira VF, Barboza EDSP. Evaluation of survival and success rates of dental implants reported in longitudinal studies with a follow-up period of at least 10 years: A systematic review. Int J Oral Maxillofac Surg. 2015;44(3):377–88. https://www.sciencedirect.com/science/article/pii/S0901502714004251
- Gallucci GO, Hamilton A, Zhou W, Buser D, Chen S. Implant placement and loading protocols in partially edentulous patients: A systematic review Clin Oral Implants Res Blackwell Munksgaard. 2018;29:106–34.
- Beagle JR. The Immediate Placement of Endosseous Dental Implants in Fresh Extraction Sites. Dent Clin North Am. 2006;50(3):375–89. https:// www.sciencedirect.com/science/article/pii/S0011853206000346
- Bhola M, Neely AL, Kolhatkar S. Immediate implant placement: Clinical decisions, advantages, and disadvantages. J Prosthodont. 2008;17(7):576– 81. https://doi.org/10.1111/j.1532-849X.2008.00359.x.
- Koh RU, Rudek I, Wang HL. Immediate implant placement: Positives and negatives. Implant Dent. 2010;19(2):98–108. https://pubmed.ncbi.nlm. nih.gov/20386212/. Cited 2021 Nov 10
- Regish KM, Sharma D, Prithviraj DR. An overview of immediate root analogue zirconia implants. J Oral Implantology. 2013;39:225–33.
- Saeidi Pour R, Freitas Rafael C, Engler MLPD, Edelhoff D, Klaus G, Prandtner O, et al. Historical development of root analogue implants: a review of published papers. Br J Oral Maxillofac Surg. 2019;57(6):496–504. https:// doi.org/10.1016/j.bjoms.2019.01.021.
- Yong LT. Single stage immediate implant placements in the esthetic zone. J Oral Implantol. 2012;38(6):738–46.
- Figliuzzi M, Mangano F, Mangano C. A novel root analogue dental implant using CT scan and CAD/CAM: Selective laser melting technology. Int J Oral Maxillofac Surg. 2012;41(7):858–62. https://doi.org/10.1016/j. iiom.2012.01.014
- Hodosh M, Povar M, Shklar G. The dental polymer implant concept. J Prosthet Dent. 1969;22(3):371–80.
- 11. Ghuneim WA. In situ tooth replica custom implant: A 3-dimensional finite element stress and strain analysis. J Oral Implantol. 2013;39(5):559–73.
- Moin D, Hassan B, Wismeijer D. Immediate Nonsubmerged Custom Root Analog Implants: A Prospective Pilot Clinical Study. Int J Oral Maxillofac Implants. 2018;33(2):e37-44.
- 13. Anssari Moin D, Hassan B, Wismeijer D. A novel approach for custom three-dimensional printing of a zirconia root analogue implant by digital light processing. Clin Oral Implants Res. 2017;28(6):668–70.
- Chen J, Zhang Z, Chen X, Zhang C, Zhang G, Xu Z. Design and manufacture of customized dental implants by using reverse engineering and selective laser melting technology. J Prosthet Dent. 2014;112(5):1088–1095.E1. https://doi.org/10.1016/j.prosdent.2014.04.026
- Mangano FG, De Franco M, Caprioglio A, MacChi A, Piattelli A, Mangano C. Immediate, non-submerged, root-analogue direct laser metal sintering (DLMS) implants: A 1-year prospective study on 15 patients. Lasers Med Sci. 2014;29(4):1321–8.
- Dantas T, Madeira S, Gasik M, Vaz P, Silva F. Customized root-analogue implants: A review on outcomes from clinical trials and case reports. Materials (Basel). 2021;14(9):1–14.
- Beuer F, Schweiger J, Edelhoff D. Digital dentistry: An overview of recent developments for CAD/CAM generated restorations. Br Dent J. 2008;204(9):505–11.
- 18. Kanazawa M, Inokoshi M, Minakuchi S, Ohbayashi N. Trial of a CAD/CAM system for fabricating complete dentures. Dent Mater J. 2011;30(1):93–6.
- Etemad-Shahidi Y, Qallandar OB, Evenden J, Alifui-Segbaya F, Ahmed KE. Accuracy of 3-dimensionally printed full-arch dental models: A systematic review. J Clinical Med MDPI. 2020;9:1–18.
- Revilla-León M, Özcan M. Additive Manufacturing Technologies Used for Processing Polymers: Current Status and Potential Application in Prosthetic Dentistry. J Prosthodont. 2019;28(2):146–58.
- Griffith ML, Halloran JW. Freeform fabrication of ceramics via stereolithography. J Am Ceram Soc. 1996;79(10):2601–8. https://doi.org/10.1111/j. 1151-2916.1996.tb09022.x.

- Moin DA, Hassan B, Mercelis P, Wismeijer D. Designing a novel dental root analogue implant using cone beam computed tomography and CAD/ CAM technology. Clin Oral Implants Res. 2013;24(A100):25–7.
- 23. Revilla-León M, Sadeghpour M, Özcan M. A Review of the Applications of Additive Manufacturing Technologies Used to Fabricate Metals in Implant Dentistry. J Prosthodont. 2020;29(7):579–93.
- Vayron R, Nguyen VH, Lecuelle B, Lomami HA, Meningaud JP, Bosc R, et al. Comparison of resonance frequency analysis and of quantitative ultrasound to assess dental implant osseointegration. Sensors (Switzerland). 2018;18(5). Available from: www.mdpi.com/journal/sensors. Cited 2022 Oct 24.
- 25. Laney. Glossary of Oral and Maxillofacial Implants. Int J Oral Maxillofac Implants. 2017;32(4):Gi-G200.
- 26. Winter W, Klein D, Karl M. Micromotion of Dental Implants: Basic Mechanical Considerations. J Med Eng. 2013;2013:1–9.
- Szmukler-Moncler S, Piattelli A, Favero GA, Dubruille JH. Considerations
  preliminary to the application of early and immediate loading protocols
  in dental implantology. Clin Oral Implants Res. 2000;11(1):12–25.
- Miri R, Shirzadeh A, Kermani H, Khajavi A. Relationship and changes of primary and secondary stability in dental implants: A review. Int J Contemp Dent Med Rev. 2017;6. https://ijcdmr.com/index.php/ijcdmr/article/viewFile/258/232
- Ivanova V, Chenchev I, Zlatev S, Mijiritsky E. Correlation between primary, secondary stability, bone density, percentage of vital bone formation and implant size. Int J Environ Res Public Health. 2021;18(13):6994.
- Tobar-Reyes J, Andueza-Castro L, Jiménez-Silva A, Bustamante-Plaza R, Carvajal-Herrera J. Micromotion analysis of immediately loaded implants with Titanium and Cobalt-Chrome superstructures. 3D finite element analysis. Clin Exp Dent Res. 2021;7(4):581–90.
- 31. Wilhelm R, Hasan I, Keilig L, Heinemann F, Stark H, Bourauel C. Biomechanical investigations of the secondary stability of commercial short dental implants in porcine ribs. Biomed Tech. 2014;59(6):507–13.
- Keilig L, Bourauel C, Grüner M, Hültenschmidt R, Bayer S, Utz KH, et al. Aufbau und Erprobung eines neuartigen Meßsystems für die dentale Biomechanik - Meßprinzip und Beispielmessungen des Hexapod-Meß-Systems. Biomed Tech. 2004;49(7–8):208–15.
- Hasan I, Heinemann F, Schwegmann M, Keilig L, Stark H, Bourauel C. Experimental investigation of commercial small diameter dental implants in porcine mandibular segments. Biomed Tech. 2017;62(1):103–8.
- Aldesoki M, Keilig L, Dörsam I, Evers-Dietze B, Elshazly TM, Bourauel C. Trueness and precision of milled and 3D printed root-analogue implants: A comparative in vitro study. J Dent. 2023;130:104425 (December 2022). https://doi.org/10.1016/j.jdent.2023.104425.
- 35. Tribst JPM, Dal Piva AM de O, Blom EJ, Kleverlaan CJ, Feilzer AJ. Dental biomechanics of root-analog implants in different bone types. J Prosthet Dent. 2022;1–11. https://doi.org/10.1016/j.prosdent.2022.10.005
- Niinomi M. Biologically and mechanically biocompatible titanium alloys. Mater Trans. 2008;49(10):2170–8.
- 37. Van Oers RFM, Feilzer AJ. Abutment-to-fixture load transfer and periimplant bone stress. Am J Dent. 2015;28(5):247–50.
- Gattinger J, Bullemer CN, Harrysson OLA. Patient specific root-analogue dental implants – Additive manufacturing and finite element analysis. Curr Dir Biomed Eng. 2016;2(1):101–4.
- Chen J, Zhang Z, Chen X, Zhang X. Influence of custom-made implant designs on the biomechanical performance for the case of immediate post-extraction placement in the maxillary esthetic zone: a finite element analysis. Comput Methods Biomech Biomed Engin. 2017;20(6):636–44. https://doi.org/10.1080/10255842.2017.1283406.

#### **Publisher's Note**

Springer Nature remains neutral with regard to jurisdictional claims in published maps and institutional affiliations.

34

## 3.3. Study 3

From model validation to biomechanical analysis: In silico study of multirooted root analogue implants using 3D finite element analysis

Mostafa Aldesoki, Ludger Keilig, Abdulaziz Alhotan, Al-Hassan Diab, Tarek M. Elshazly, Christoph Bourauel

Journal of the Mechanical Behavior of Biomedical Materials (2025)

https://doi.org/10.1016/j.jmbbm.2025.106896

Impact factor: 3.3

Contents lists available at ScienceDirect

## Journal of the Mechanical Behavior of Biomedical Materials

journal homepage: www.elsevier.com/locate/jmbbm

## From model validation to biomechanical analysis: In silico study of multirooted root analogue implants using 3D finite element analysis

Mostafa Aldesoki a,b,\* 0, Ludger Keilig a,c 0, Abdulaziz Alhotan 0, Al-Hassan Diab 0, Tarek M. Elshazly <sup>a,1</sup>, Christoph Bourauel <sup>a,1</sup>

- a Oral Technology, Dental School, University Hospital Bonn, Bonn, Germany
- Clinic for Conservative Dentistry and Periodontology, LMU Hospital, Munich, Germany
- Eppartment of Prosthetic Dentistry, Preclinical Education and Materials Science, Dental School, University Hospital Bonn, Bonn, Germany
- <sup>d</sup> Department of Dental Health, College of Applied Medical Sciences, King Saud University, Riyadh, Saudi Arabia
- <sup>e</sup> Department of Oral Medicine, Periodontology and Diagnosis, Faculty of Dentistry, British University in Egypt, Cairo, Egypt

#### ARTICLE INFO

#### Keywords: Root analogue implant (RAI) Dental implant Finite element analysis Biomechanics Abutment design Validation study

#### ABSTRACT

Objectives: To create a validated 3D finite element model and employ it to examine the biomechanical behaviour of multirooted root analogue implants (RAIs).

Methods: A validated finite element model comprising either an RAI or a threaded implant (TI) and an idealised bone block was developed based on a previously conducted in vitro study. All the experimental boundary conditions and material properties were reproduced. Force/displacement curves were plotted to ensure complete alignment with the in vitro findings. Following the validation of the FE model, the material properties were adjusted to align with those reported in the literature. Two contact scenarios were then examined: immediate placement with touching contact and osseointegration with glued contact. The bone block was constrained in all directions, and a 300 N point load was applied along the long axis of the implant, and with an angulation of 30°. The resulting values for equivalent stress, maximum principal stress, microstrain, and displacement were evaluated.

Results: The numerical model demonstrated a high degree of agreement with the experimental results, particularly regarding displacement in the loading direction (Z). The findings of the applied FEA indicated that RAIs generally outperformed TIs. The RAI exhibited lower equivalent stress, with values of 3.3 MPa for axial loading and 13.1 MPa for oblique loading, compared to 5.4 MPa and 29.5 MPa for the TI, respectively. Furthermore, microstrain was observed to be lower in the RAI, with a value of 4,000 με compared to 13,000 με in the TI under oblique loading. Additionally, the RAI exhibited superior primary and secondary stability, with lower micromotion values compared to the TL

Conclusions: The root analogue implant showed superior biomechanical performance, with more uniform stress distribution and greater stability compared to the conventional threaded implant, positioning it as a promising alternative.

#### 1. Introduction

Dental implants present an appealing choice for the replacement of missing teeth, offering numerous benefits in terms of reliability and comfort, thereby enhancing one's quality of life (Baldi et al., 2018). Immediate implants refer to implants that are placed immediately following surgical extraction of non-restorable teeth (Koh et al., 2010).

The fundamental idea behind immediate implant placement is to maintain the height and width of the alveolar bone, thus minimizing the common occurrence of bone loss around the extraction site during the healing process (Beagle, 2006; Bhola et al., 2008). The benefit of immediate implants encompasses the elimination of the necessity for a subsequent surgical intervention, consequently leading to a reduced overall treatment duration (Beagle, 2006).

https://doi.org/10.1016/j.jmbbm.2025.106896

Received 14 October 2024; Received in revised form 18 December 2024; Accepted 12 January 2025 Available online 18 January 2025

1751-6161/© 2025 The Authors. Published by Elsevier Ltd. This is an open access article under the CC BY-NC license (http://creativecommons.org/licenses/bync/4.0/).

<sup>\*</sup> Corresponding author: Oral Technology, University Hospital Bonn, Welschnonnenstr. 17, 53111 Bonn, Germany. E-mail addresses: aldesoki@uni-bonn.de (M. Aldesoki), ludger.keilig@uni-bonn.de (L. Keilig), aalhotan@ksu.edu.sa (A. Alhotan), alhassan.diab@bue.edu.eg (A.-H. Diab), tarek.m.elshazly@gmail.com (T.M. Elshazly), bourauel@uni-bonn.de (C. Bourauel).

<sup>&</sup>lt;sup>1</sup> These co-authors contributed equally to the manuscript and shared the last authorship.

Recent advancements in digital dentistry including the continuous progress in cone beam computed tomography (CBCT) and computer-aided design/computer-aided manufacturing (CAD/CAM) technologies have paved the way for the utilization of personalized patient-specific root analogue implants (RAIs) (Böse et al., 2020; Figliuzzi et al., 2012). The concept of RAI was initially introduced by Hodosh et al., in 1969, utilizing a heat-processed methyl methacrylate implant. However, this method faced setbacks due to its inability to achieve osseointegration (Hodosh et al., 1969). A reintroduction of the technique in 1992, substituting the polymer with pure titanium, led to successful osseointegration (Saeidi Pour et al., 2019).

The concept of the RAI involves replacing a tooth scheduled for extraction through immediate implant placement. The RAI is designed to match the original root anatomy based on CBCT data, ensuring precise congruence with the empty socket, an advantage not offered by TI (Moin et al., 2018). This approach is anticipated to enhance primary stability while minimizing bone and soft tissue trauma in comparison to conventional threaded implants (TI) (Regish et al., 2013). Moreover, expected additional advantages encompass straightforward placement, immediate soft tissue support, and a reduction in the number of required surgeries (Anssari Moin et al., 2017; Chen et al., 2014). However, potential limitations of RAIs include the complexity and high cost of design and fabrication, challenges in achieving a precise fit, and a lack of extensive clinical data to validate their long-term efficacy (Moin et al., 2013).

A critical determinant of the successful osseointegration of dental implants is the implant stability (Ivanova et al., 2021). Implant stability is a term defined as the absence of clinical implant mobility and is categorized into primary and secondary stability (Sennerby and Meredith, 2008). Primary stability is attained through the mechanical anchoring of the implant during the initial insertion, while secondary stability evolves as a consequence of subsequent bone remodelling and complete bone healing. Accordingly, primary stability is regarded as a mechanical phenomenon, whereas secondary stability is a biological process driven by osseointegration (Miri et al., 2017).

Finite Element Analysis (FEA) stands as a numerical method employed to model complex physical systems (Falcinelli et al., 2023). The underlying principle of FEA involves the simplification of intricate and irregular structures by creating a mesh consisting of a finite number of elements interconnected by nodes (Elshazly et al., 2023b; Fiorillo et al., 2022). Within dental research, FEA offers the advantage of examining biomechanical structures that might be challenging to investigate either *in vivo* or *in vitro*. Additionally, it facilitates the study of various materials and designs without incurring additional costs (Aldesoki et al., 2022; Wang et al., 2022).

The American Society of Mechanical Engineers (ASME) defines verification as the process to ensure that the computational model accurately fits the mathematical description, whereas it defines validation as the process to confirm that the model accurately represents the real-world application. In other words, validation is the process of comparing computational predictions with experimental data or the real system (Anderson et al., 2007; Chang et al., 2018).

The aim of this study was to develop a validated 3D numerical finite element model based on previous *in vitro* research (Aldesoki et al., 2024), and to use this model to investigate the biomechanical behaviour of multirooted RAIs. The research hypothesis postulated that there is no difference in terms of biomechanical behaviour between the multirooted RAI and the conventional TI.

#### 2. Material and methods

#### 2.1. Study design

In this study, we have developed a validated finite element model based on experimental data from previous *in vitro* study (Aldesoki et al., 2024). This model is used to compare the biomechanical properties of

the RAI with those of the conventional TI, which serves as the control.

#### 2.2. Model validation

#### 2.2.1. Data acquisition & models generation

To obtain a digital replica of the experimental model, a CBCT (Cone Beam Computed Tomography) scan of a dentate mandible was imported into a 3D medical image processing software (Mimics 25; Materialise, Leuven, Belgium) for manual segmentation. The scanning parameters were as follows: accelerating voltage of 90 kV, beam current of 12 mA, and resolution of 75  $\mu m$ . The total scanning time was 15 s, and a total of 668 slices were scanned for modelling.

Tooth 47 was segmented by assigning a minimum and a maximum threshold based on histogram analysis. Subsequently, the segmented tooth was exported to a meshing software (3-matic 17; Materialise, Leuven, Belgium) to finalise the design of the RAI based on the anatomy of the tooth. The RAI included a coronal portion designed as an idealised cube with a side length of 5 mm, as specified in the *in vitro* study. Its mesial root measured 15 mm in length, whereas the distal root measured 14 mm. The buccolingual and mesiodistal dimensions were approximately 10 mm (Fig. 1).

Regarding the TI, the CAD model of the exact implant utilized in the  $\it in~vitro$  study (Ankylos 4.5  $\times$  11 mm; Dentsply-Friadent, Mannheim, Germany) was imported into 3-matic software (Fig. 1). Subsequently, a rectangular bone block was designed in 3-matic based on the shape of the artificial bone block used in the experimental study. The cortical bone was 2 mm in height, 20 mm in length, and 20 mm in width, whereas the trabecular bone was 33 mm in height, 20 mm in length, and 20 mm in width.

Lastly, a spoon-shaped attachment was designed to closely resemble the loading conditions in the Hexapod Measurement System (HexMeS), a self-developed set-up designed for applications in dental biomechanics (Keilig et al., 2004). This attachment serves as a lever arm which is attached to the hexapod robot at one side and connected to the implant specimen at the other side so that any movement in the hexapod could be transmitted as an applied load on the implant, which is recorded by a force/torque sensor (Fig. 2A and B).

#### 2.2.2. Mesh generation

In 3-matic, a non-manifold assembly of the implant, the cortical bone, and the trabecular bone was created. This assembly is a crucial step when performing an FEA with multiple structures, which are intersecting with each other. Afterward, to optimize and locally refine the surface mesh while preserving the detailed features, an adaptive

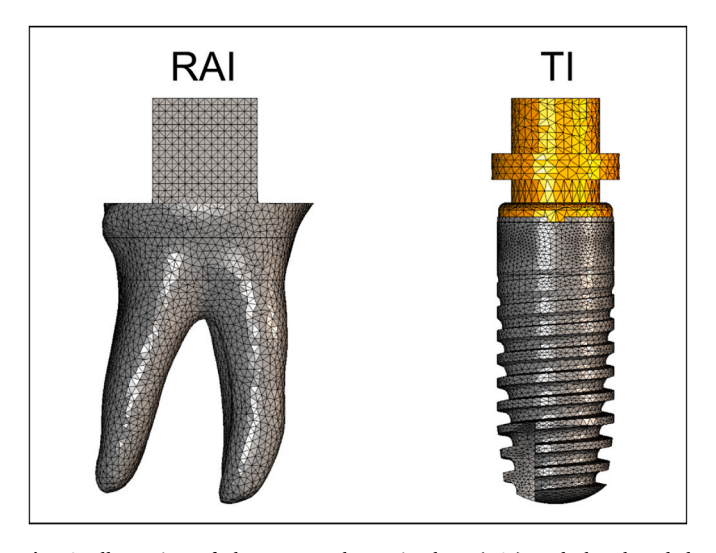
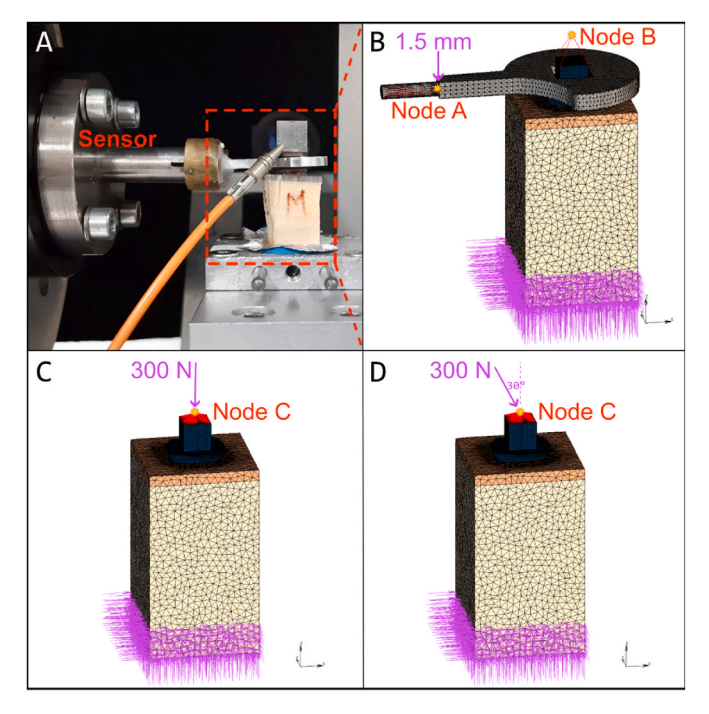


Fig. 1. Illustration of the root analogue implant (RAI) and the threaded implant (TI).



**Fig. 2.** Illustration of the finite element (FE) models with the specified boundary conditions. A. The Hexapod Measurement System (HexMeS). B. FE Validation model. C. FE applied model illustrating the axial loading. D. FE applied model illustrating the oblique loading.

triangular meshing was applied to the assembly with a maximum element size of 0.5 mm. Skewness was selected as a shape-measure parameter, and the maximum geometrical error was set to 0.05 mm. Finally, the triangular surface mesh was converted into a volume mesh, in which a volume mesh consisting of up to 96,969 4-noded tetrahedral elements (Tetra 4) was generated and exported in Abaqus format to an FE preprocessing and postprocessing software (Marc Mentat, 2020; MSC Software, Los Angeles, California, USA) for the FE analysis.

#### 2.2.3. Material properties, contact bodies

In Marc Mentat, the material properties were assigned based on the elastic modulus and Poisson's ratio. According to many studies conducted on oral hard tissue (Aldesoki et al., 2022; Elshazly et al., 2023a; Tribst et al., 2024), all materials were assumed to be linear, homogenous, elastic, and isotropic. For the validation model, a sensitivity analysis was done to select the optimum material properties that best represent the properties of the artificial bone used in the experimental study (Sawbones; Pacific Research Laboratories, Vashon, USA). Starting from the normal elastic modulus values reported in the literature (13, 700 MPa and 1,370 MPa for cortical and trabecular bone, respectively), the best results were obtained by applying the Sawbones material properties listed by the manufacturer (Table 1). All components were defined as deformable contact bodies, and the contact interaction between the contact bodies was defined through a contact table. Glued interaction was assigned between the implant and the bone indicating full osseointegration, whereas a touching sliding contact interaction was

**Table 1**Material properties assigned to various components in the finite element model.

Material	Elastic modulus (GPa)	Poisson's ratio
Titanium (TI and RAI)	110.0	0.35
Aluminium (spoon attachment)	70.0	0.32
Cortical bone	13.7	0.30
Trabecular bone	1.37	0.30
Sawbones - Cortical	17.0	0.26
Sawbones - Trabecular	0.058	0.30

assigned between the spoon-shaped attachment and the implant with a friction coefficient of 0.34.

#### 2.2.4. Boundary conditions and load application

To validate the model, we aimed to accurately reproduce the boundary conditions and the loading protocol in the experimental study. Hence, the nodes of the lower border of the bone block were constrained for translation and rotation in X, Y, and Z directions. Additionally, the so-called rigid body elements (RBE2) were used in which 127 tied nodes at the proximal end of the spoon were selected and connected in turn to a reference central node "Node A" at the exact location of the force/torque sensor in the experimental setup. This reference node was used to apply a 1.5 mm translation in the negative Z direction. This translation will, consequently, act as an indirect load on the surface of the implant (Fig. 2B).

### 2.2.5. FEA output and post-processing

Regarding the FEA output, force values were recorded at node A for all increments. Additionally, a new RBE2 was created in which 4 tied nodes at the top surface of the implant were connected to a central reference node "Node B", 5 mm above the implant surface, which represents the same point for recorded displacements in the experimental setup as shown in Fig. 2A and B. At this node, total displacement, as well as displacement in the Z axis were assessed for all increments and consequently, history plots of force/displacement curves were plotted.

#### 2.3. Applied finite element analysis

Once the FE model had been validated, new simulations were conducted to study and compare the biomechanical behaviour of RAI and TI. For this purpose, the validated model was used without including the spoon attachment. The material properties of bone were modified to the values reported in the literature as shown in Table 1. Additionally, two different contact cases were utilized; an immediate implant placement case with touching contact interaction between the implant and the bone contact bodies with a friction coefficient of 0.71 (Falcinelli et al., 2023; Tobar-Reyes et al., 2021), and a complete osseointegration case with glued contact interaction between the implant and the bone. As a boundary condition, the lower border of the bone cube was constrained for translation and rotation in X, Y, and Z directions. The implant was loaded according to the ISO standard 14801, where a new RBE2 reference node (Node C) was created 8 mm above the bone surface. Consequently, all the nodes at the top surface of the implant were selected as tied nodes to this node so that any applied load on the reference node would be evenly distributed along the tied nodes. Finally, a 300 N point load was applied to node C, directed along the long axis of the implant, and with an angulation of 30° to the long axis from the buccal to the lingual direction (Fig. 2C and D).

#### 3. Results

### 3.1. Validation model

A strong agreement was observed between the results of the numerical and experimental models. The history plots at the reference nodes were validated by the load-displacement curves from the experimental study, as illustrated in Fig. 3. Regarding the maximum displacements at a force of 50 N, comparable displacement (Z) values were noted for both the RAI and TI models in both numerical and experimental analyses. This agreement also extended to the total displacement values for the TI model. However, a discrepancy was observed when comparing the numerical and experimental total displacement values for the RAI model.

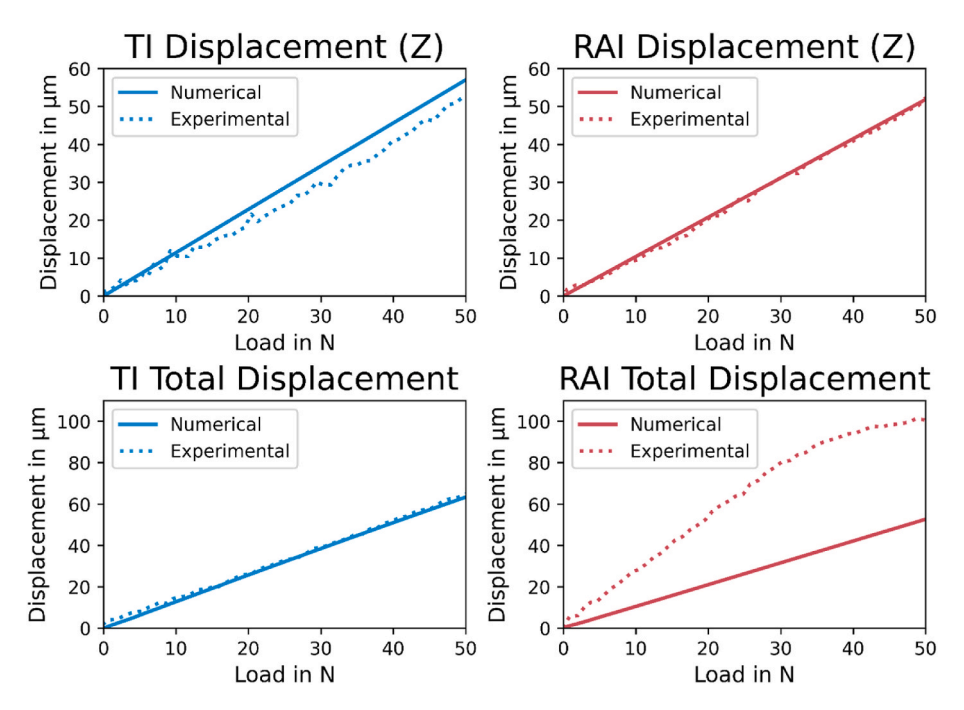


Fig. 3. Line chart illustrating the load-displacement curves for TI and RAI in both numerical and experimental models.

#### 3.2. Applied FEA

After validation, two stages of healing were investigated: the immediate placement stage, prior to osseointegration, and the osseointegration stage. In both stages, stress, strain, and displacement values were evaluated under both axial and oblique loading conditions.

## 3.2.1. Immediate placement stage

The TI model exhibited notably higher equivalent stress compared to the RAI model, with stress values three times greater under axial loading and four times greater under oblique loading (Table 2). Stress distribution, as shown by the coloured contour bands, revealed concentration at the abutment and cervical region of the fixture in the TI model for both loading conditions. In contrast, the RAI model displayed a more uniform stress distribution along the bone-implant interface (Figs. 4 and 5).

In terms of stress distribution within the supporting bone structure, the TI model exhibited higher equivalent stress than the RAI model under both axial and oblique loading. Maximum principal stress (tensile stress) increased slightly in the TI model under axial loading (5.4 MPa vs. 3.3 MPa for RAI), and more significantly under oblique loading (29.5 MPa vs. 13.1 MPa for RAI). In axial loading, tensile stress was concentrated at the cortical-trabecular bone junction and the implant threads in the TI model, while it was more evenly distributed in the RAI model. Under oblique loading, tensile stress was concentrated at the proximal cortical bone surface, especially in the TI model, as shown in Figs. 5 and 6.

A slight difference in bone microstrain ( $\mu\epsilon$ ) was observed under axial

loading, with 5,000  $\mu\epsilon$  for TI and 4,000  $\mu\epsilon$  for RAI. Under oblique loading, microstrain increased significantly in TI (13,000  $\mu\epsilon$ ), while remaining at 4,000  $\mu\epsilon$  in RAI. In TI, the elevated microstrain was concentrated at the cervical buccal wall and apical lingual wall, reflecting implant rotation under oblique load (Figs. 5 and 7).

Evaluating the primary stability by measuring the micromotion (displacement) in the TI and the RAI revealed that the RAI was better in the primary stability under both axial and oblique loading (Table 3, Fig. 8).

### 3.2.2. Osseointegrated stage

The equivalent stress values and distribution in the implant were unaffected by osseointegration for both TI and RAI (Table 2, Figs. 4 and 5). In bone, under axial loading, stress remained around 8.0 MPa for TI but decreased by half in RAI to 2.9 MPa. Under oblique loading, stresses dropped notably in both models, with TI showing 30.4 MPa and RAI one-third of that at 10.0 MPa.

In terms of maximum principal stress (tensile stress) in bone, osseointegration had little effect under axial loading, while in oblique loading, it dropped to 23.9 MPa for TI and 6.1 MPa for RAI. Initially concentrated at the TI threads, tensile stress shifted to the cortical-trabecular bone junction after osseointegration (Fig. 6).

Bone microstrain ( $\mu\epsilon$ ) under axial loading was 3,000  $\mu\epsilon$  for TI and 2,000  $\mu\epsilon$  for RAI. Under oblique loading, TI had a higher strain at 7,000  $\mu\epsilon$  compared to 4,000  $\mu\epsilon$  for RAI. Microstrain decreased overall compared to the immediate placement stage, except for RAI under oblique loading (Figs. 5 and 7).

Similar to primary stability, RAI showed better secondary stability

**Table 2**Peak equivalent stress, tensile stress, and microstrain under axial and oblique loading conditions.

Loading type	Healing condition	Equivalent	Equivalent stress in MPa				Tensile stress in MPa		Microstrain (με)	
		Implant		Bone		Bone		Bone		
		TI	RAI	TI	RAI	TI	RAI	TI	RAI	
Axial load	Immediate placement	85.3	24.6	8.5	5.5	5.4	3.3	5,000	4,000	
	Osseointegration	84.7	24.0	8.1	2.9	5.4	2.3	3,000	2,000	
Oblique load	Immediate placement	392.2	87.7	42.4	20.6	29.5	13.1	13,000	4,000	
	Osseointegration	389.8	85.4	30.4	10.1	24.0	6.2	7,000	4,000	

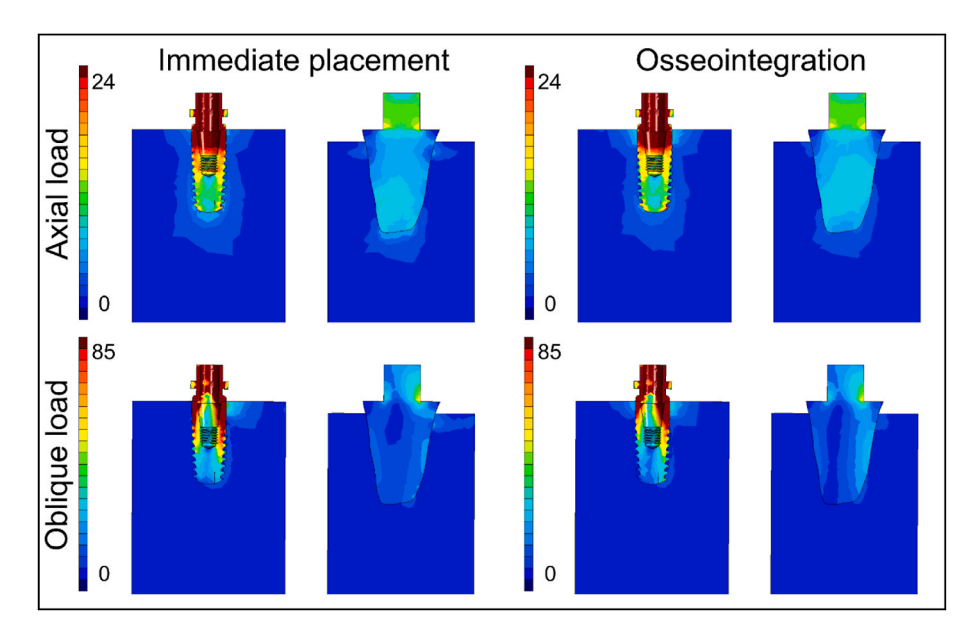


Fig. 4. Equivalent stress distribution in MPa in immediately placed and osseointegrated TI and RAI under axial and oblique loading conditions.

than TI under both loading conditions. Micromotion values under axial loading were 22  $\mu$ m for TI and 16  $\mu$ m for RAI, and under oblique loading, 191  $\mu$ m for TI and 165  $\mu$ m for RAI (Table 3, Fig. 8).

#### 4. Discussion

Long-term outcomes of RAIs show promising results, with studies highlighting their potential for high survival rates and satisfactory osseointegration. Recent evaluations indicate survival rates comparable to conventional implants, ranging from 90% to 95% over follow-up periods extending beyond a year. For instance, RAIs customised via CAD/CAM and advanced manufacturing techniques have demonstrated excellent stability and minimal marginal bone loss, emphasizing their suitability for maintaining peri-implant tissue health over time (Böse et al., 2020; Figliuzzi et al., 2022).

Despite the significant advancements in the design and application of customized RAIs, the available literature on RAIs is still limited (Dantas et al., 2021). This *in silico* study aims to evaluate the biomechanical behaviour of multirooted RAIs using a validated 3D FE model. Based on the performed biomechanical analysis, the RAI demonstrated superior stress distribution and stability compared to the conventional TI. Hence, the study's hypothesis was rejected.

Recently, FEA has proven to be exceptionally valuable in studying biological structures and tissues under various simulations. Specifically, FEA allows for the evaluation of stresses at the bone-implant interface during mastication (Chang et al., 2018; Maminskas et al., 2016). Dumont et al. (2009) highlighted the necessity of experimentally validating FEA studies involving biological tissues. Similarly, Chang et al. (2018) strongly recommended for clearly indicating the model's validation process when presenting a finite element study. Hence, to achieve precise validation, this study utilized experimental data from a previous *in vitro* study (Aldesoki et al., 2024) to validate the numerical model. This was achieved by precisely reproducing the experimental setup conditions and comparing the resultant displacements under identical loading conditions.

Since the RAI can only be used as an immediate implant to replace an existing non-restorable tooth (Moin et al., 2018), CBCT data was utilized to design the RAI based on the anatomical shape of tooth 47 (Aldesoki et al., 2023). A multirooted tooth was selected to study the complex biomechanical behaviour owing to the distinctive shape and orientation of its two roots. The spoon-shaped attachment was modelled to replicate the same loading mode used in the experimental setup, where the

implant is indirectly loaded by the downward movement of the spoon. This step was crucial to accurately simulate the lever effect acting on the implant.

Titanium alloy was selected as the material of choice for TI and RAI based on many previous studies (Moin et al., 2013; Tribst et al., 2024; Wang et al., 2022). Glued contact interaction was assumed for the validation model following the *in vitro* study (Aldesoki et al., 2024). In the applied FEA, two healing conditions were simulated to comprehensively assess biomechanical behaviour. A touching contact interaction was used to represent the unhealed condition of an immediately placed implant, while a glued contact interaction simulated the healed condition of an osseointegrated implant (Lundgren et al., 1992).

Most finite element studies have considered static loads ranging from 200 N to 600 N for the molar area (Falcinelli et al., 2023; Fiorillo et al., 2022; Tribst et al., 2024; Wang et al., 2022). To select a specific value, sensitivity tests were carried out with a static load of up to 600 N applied in six increments. The monitored displacement and stress values increased linearly with each increment. Consequently, a static load of 300 N was selected and applied axially and at a 30° angle to the long axis, following ISO standard 14801 and previous studies (Büyük et al., 2022; Falcinelli et al., 2023; Pessanha-Andrade et al., 2018), to encompass all loading conditions on the implant.

The load-displacement curves of the numerical model aligned well with the experimental results, except for a noticeable discrepancy in the total displacement curves of the RAI model. This difference likely stems from the standardised FEA simulation conditions versus operator variability in the experimental setup. Specifically, the RAI was manually inserted into a socket-shaped cavity in the Sawbones block, unlike the TI, which followed the manufacturer's surgical protocol for insertion (Aldesoki et al., 2024). The technique-sensitive insertion of the RAI makes it challenging to align it perfectly within the Sawbones block without any angulation given the asymmetrical RAI roots, potentially increasing the non-axial displacement components due to uneven contact between the spoon attachment and the top surface of the RAI.

Regarding the applied FEA, the equivalent stress under oblique loading was about 4.5 times higher than axial loading for the TI, and 3.5 times higher for the RAI. Total displacement under oblique loading was approximately nine times greater for both implants. Overall, the RAI performed better, showing a more uniform stress distribution and an equivalent stress nearly three times lower than the TI. This can be attributed to the RAI's larger surface area (Dantas et al., 2020; Tribst et al., 2024; Wang et al., 2022) and its multirooted design (Wang et al.,

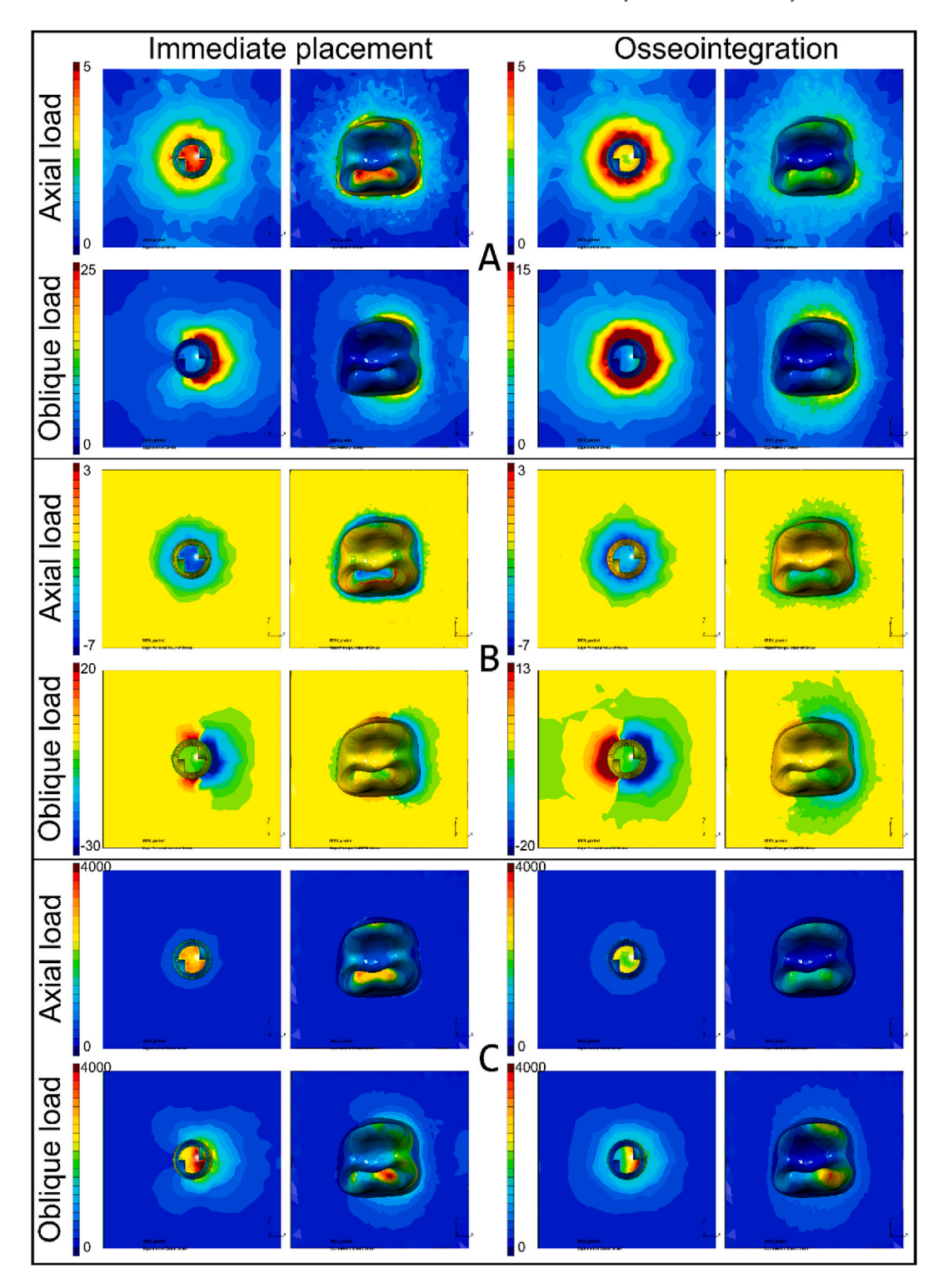


Fig. 5. Top view of immediately placed and osseointegrated TI and RAI under axial and oblique loading conditions. A. Equivalent stress in MPa. B. Maximum principal stress (Tensile) in MPa. C. Microstrain.

2022), which better dissipates masticatory loads and distributes stress more evenly, reducing stress concentrations as shown by the contour bands.

These findings are consistent with Tribst et al. (2024), who used FEA to show that zirconia RAIs outperform conventional screw-shaped implants in dissipating masticatory loads. Another FEA study (Dantas et al., 2020) examined the induced stress fields around RAI and conventional threaded zirconia implants, and concluded that RAIs promoted a

superior stress distribution in compact bone compared to TIs. Wang et al. (2022) compared the biomechanical behaviour of six RAIs with different root shapes to a tapered TI, concluding that RAIs significantly reduce stress under identical loading conditions. Such conclusion was confirmed by another FEA study by Nimmawitt et al. (2022) who stated that the stress distribution in the RAI was more favourable than the TI at the bone-implant interface in all implant types.

According to Frost's Mechanostat hypothesis (Frost, 2003), bone

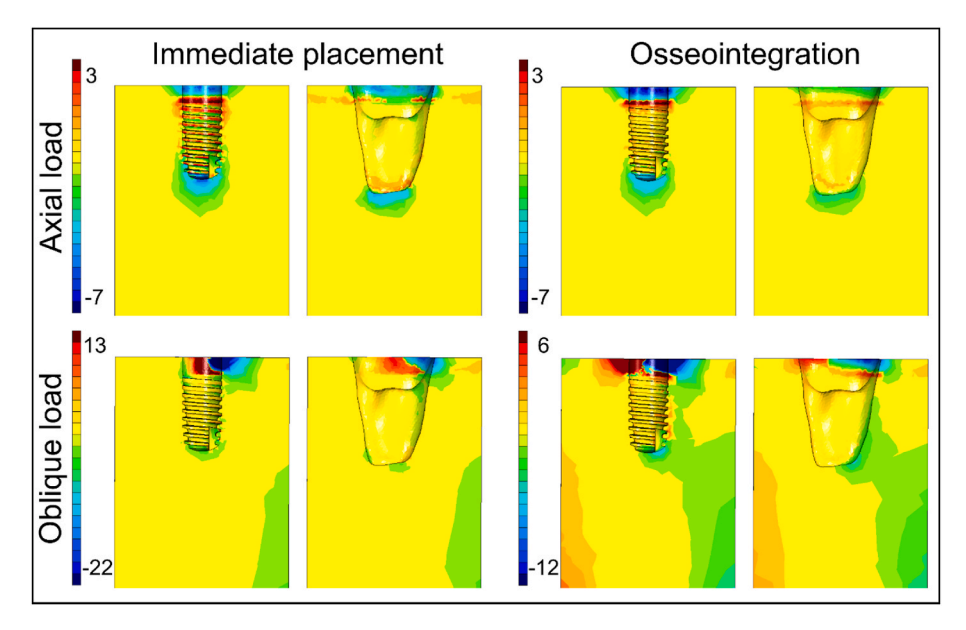


Fig. 6. Maximum principal stress distribution (tensile) in MPa in immediately placed and osseointegrated TI and RAI under axial and oblique loading conditions.

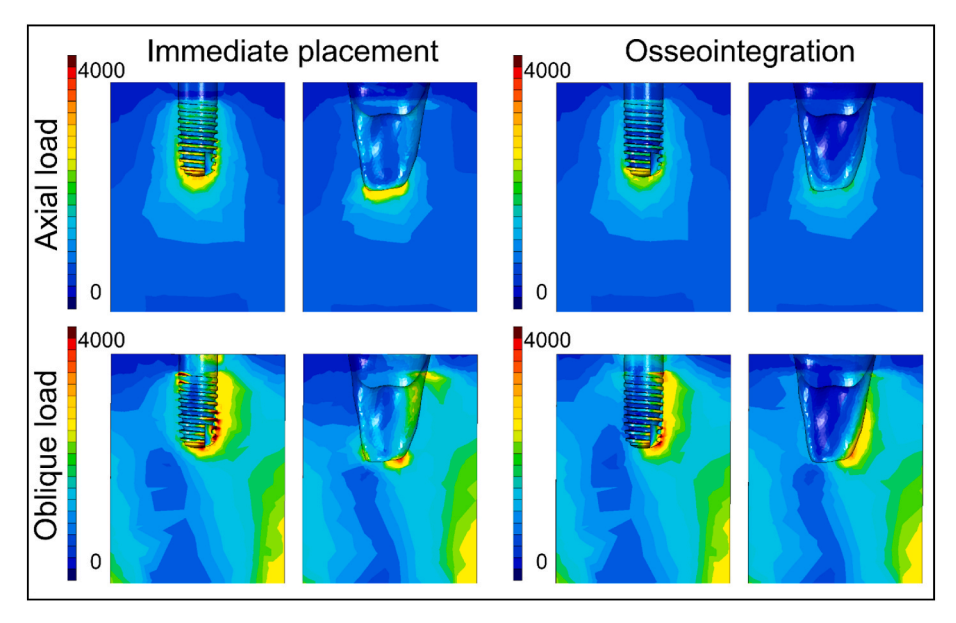


Fig. 7. Microstrain distribution in immediately placed and osseointegrated TI and RAI under axial and oblique loading conditions.

**Table 3**Maximum displacement of TI and RAI under axial and oblique loading conditions.

Loading type	Healing condition	Displacem	Displacement in µm							
		X	X		Y		Z		Total	
		TI	RAI	TI	RAI	TI	RAI	TI	RAI	
Axial load	Immediate placement Osseointegration	0	2 2	1	2 2	24 22	19 16	24 22	20 16	
Oblique load	Immediate placement Osseointegration	199 186	177 162	2	1 1	53 50	52 45	204 191	181 165	

adapts its strength and density in response to mechanical load. In the disuse range (<50–100  $\mu\epsilon$ ), inadequate loading leads to bone resorption and possible osteoporosis. The adapted range (100–2,500  $\mu\epsilon$ ) reflects typical daily activity, maintaining a balance between bone formation and resorption. In the physiological overload range (2,500–4,000  $\mu\epsilon$ ), bone formation is stimulated Strains exceeding 4,000  $\mu\epsilon$  fall into the

pathological overload range, likely causing bone damage and fractures. Our analysis showed that microstrain values after osseointegration fell within the physiological overload range for both the TI and RAI under axial loading. However, under oblique loading, the TI displayed significantly higher microstrain values in the pathological overload range, reaching 13,000  $\mu\epsilon$  at immediate loading and dropping to 7,000  $\mu\epsilon$ 

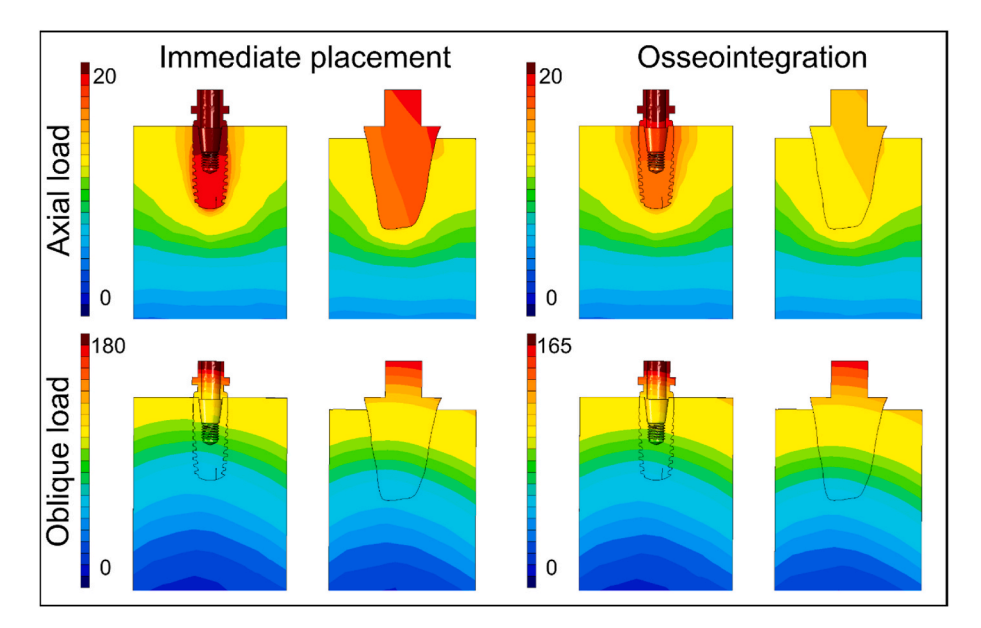


Fig. 8. Total displacement distribution in µm in immediately placed and osseointegrated TI and RAI under axial and oblique loading conditions.

post-osseointegration, in agreement with previous studies (Dantas et al., 2020; Tribst et al., 2024).

RAIs have promising clinical applications, particularly in cases requiring immediate implant placement, where preserving the natural socket anatomy is essential. Their custom-fit design allows for better adaptation to the extraction site compared to TIs, potentially minimizing the need for bone grafting and reducing surgical trauma (Anssari Moin et al., 2017; Chen et al., 2014). This anatomical congruence may contribute to enhanced primary stability and improved soft tissue outcomes, offering a less invasive alternative for patients. However, the clinical success of RAIs is highly dependent on patient-specific factors, including bone quality, cortical thickness, and socket morphology (Regish et al., 2013). Furthermore, their performance can be significantly influenced by the surgical technique and operator expertise, both of which are crucial for achieving optimal primary and secondary stability (Moin et al., 2013).

Implant stability, both immediately after placement and post-osseointegration, is critical for success. It is essential to keep micromotion within the accepted biological range to ensure proper healing and osseointegration (Vayron et al., 2018). Excessive micromotion at the bone-implant interface, especially beyond 150  $\mu m$ , can hinder healing, leading to fibrous tissue formation instead of bone, which compromises implant stability and long-term success of the implant (Szmukler-Moncler et al., 2000; Winter et al., 2013).

Similar to the studies reported by Gattinger et al. and Dantas et al. (Dantas et al., 2020; Gattinger et al., 2016), our findings show that the RAI offers superior primary and secondary stability compared to the TI. This is evident from its reduced displacement under both axial and oblique loading and in both contact conditions. This can be directly attributed to the increased surface area of the RAI, which improves both primary and secondary stability (Heimes et al., 2023; Javed et al., 2013), and to the multirooted design, which renders it more stable under axial and oblique loading (Wang et al., 2022). It is noteworthy that displacement under oblique loading was about 10 times greater than that under axial loading, primarily along the X-axis, corresponding to the lingually directed load. Although these displacements exceeded 150 µm, they should not hinder osseointegration, as they represent the combined movement of the implant and supporting bone and not the relative micromotion at the implant-bone interface.

While this 3D finite element study leverages advanced CAD/CAM technologies to design RAIs tailored to the original root anatomy and provides valuable biomechanical insights by validating an FE model

against experimental data, several limitations must be acknowledged. First, the FEA simulations were based on idealised conditions that may not fully reflect the complexities of an *in vivo* environment, such as bone quality, patient variability, and biological responses. Additionally, the material properties used were assumed to be homogeneous and isotropic, which does not accurately represent the anisotropic nature of bone and other tissues. Lastly, despite validation against *in vitro* data, discrepancies may arise due to inherent differences between computational models and real-world conditions.

Future research will focus on evaluating RAIs constructed from various materials and designs under different loading conditions. It is recommended that subsequent studies enhance the current model by integrating more clinically relevant material properties for both the bone and the implant. Additionally, the relative micromotion at the implant-bone interface will be investigated in future studies. Moreover, experimental and numerical investigations should be complemented by well-designed clinical studies to validate the findings.

## 5. Conclusion

The validated FEA model provides a reliable tool for predicting the biomechanical behaviour of dental implants. Based on the outcomes of the current validated model, the following conclusions can be drawn.

- The RAI demonstrated superior biomechanical performance and a more uniform stress distribution compared to the conventional TI.
- The RAI exhibited higher stability under both axial and oblique loading conditions, making it a promising alternative to conventional implants.

#### CRediT authorship contribution statement

Mostafa Aldesoki: Writing – original draft, Visualization, Methodology, Investigation, Formal analysis, Data curation, Conceptualization. Ludger Keilig: Writing – review & editing, Visualization, Software, Methodology, Investigation, Data curation. Abdulaziz Alhotan: Writing – review & editing, Resources. Al-Hassan Diab: Writing – review & editing, Investigation, Data curation. Christoph Bourauel: Writing – review & editing, Validation, Supervision, Project administration.

#### Informed consent statement

Not Applicable.

#### Compliance with ethics requirements

This article does not contain any studies with human or animal subjects.

#### Institutional review board statement

Not Applicable.

#### **Funding**

This work was supported by a grant from the German Academic Exchange Service (DAAD, 2019/20, 57440921).

#### Declaration of competing interest

The authors declare that they have no known competing financial interests or personal relationships that could have appeared to influence the work reported in this paper.

## Acknowledgements

The authors thank the Researchers Supporting Project Number (RSPD2025R790), King Saud University, Riyadh, Saudi Arabia.

#### Data availability

Data will be made available on request.

#### References

- Aldesoki, M., Bourauel, C., Elshazly, T.M., Schkommodau, E., Keilig, L., 2024. Evaluation of micromotion in multirooted root analogue implants embedded in synthetic bone blocks: an in vitro study. BMC Oral Health 24, 1–9. https://doi.org/10.1186/ s12903-024-03854-1.
- Aldesoki, M., Bourauel, C., Morsi, T., El-Anwar, M.I., Aboelfadl, A.K., Elshazly, T.M., 2022. Biomechanical behavior of endodontically treated premolars restored with different endocrown designs: finite element study. J. Mech. Behav. Biomed. Mater. 133, 105309. https://doi.org/10.1016/j.jmbbm.2022.105309.
- Aldesoki, M., Keilig, L., Dörsam, I., Evers-Dietze, B., Elshazly, T.M., Bourauel, C., 2023. Trueness and precision of milled and 3D printed root-analogue implants: a comparative in vitro study. J. Dent. 130, 104425. https://doi.org/10.1016/j. jdent.2023.104425.
- Anderson, A.E., Ellis, B.J., Weiss, J.A., 2007. Verification, validation and sensitivity studies in computational biomechanics. Comput. Methods Biomech. Biomed. Eng. 10, 171–184. https://doi.org/10.1080/10255840601160484.
- Anssari Moin, D., Hassan, B., Wismeijer, D., 2017. A novel approach for custom three-dimensional printing of a zirconia root analogue implant by digital light processing. Clin. Oral Implants Res. 28, 668–670. https://doi.org/10.1111/clr.12859.
- Baldi, D., Lombardi, T., Colombo, J., Cervino, G., Perinetti, G., Di Lenarda, R., Stacchi, C., 2018. Correlation between insertion torque and implant stability quotient in tapered implants with knife-edge thread design. BioMed Res. Int., 7201093 https://doi.org/10.1155/2018/7201093, 2018.
- Beagle, J.R., 2006. The immediate placement of endosseous dental implants in fresh extraction sites. Dent. Clin. 50, 375–389. https://doi.org/10.1016/j. cden.2006.03.003.
- Bhola, M., Neely, A.L., Kolhatkar, S., 2008. Immediate implant placement: clinical decisions, advantages, and disadvantages. J. Prosthodont. 17, 576–581. https://doi. org/10.1111/j.1532-849X.2008.00359.x.
- Böse, M.W.H., Hildebrand, D., Beuer, F., Wesemann, C., Schwerdtner, P., Pieralli, S., Spies, B.C., 2020. Clinical outcomes of root-analogue implants restored with single crowns or fixed dental prostheses: a retrospective case series. J. Clin. Med. 9, 1–19. https://doi.org/10.3390/jcm9082346.
- Büyük, F.N., Savran, E., Karpat, F., 2022. Review on finite element analysis of dental implants. J. Dent. Implant Res. 41, 50–63. https://doi.org/10.54527/ idir 2022 41 3 50
- Chang, Y., Tambe, A.A., Maeda, Y., Wada, M., Gonda, T., 2018. Finite element analysis of dental implants with validation: to what extent can we expect the model to predict biological phenomena? A literature review and proposal for classification of a validation process. Int. J. Implant Dent. 4. https://doi.org/10.1186/s40729-018-0110-5

- Chen, J., Zhang, Z., Chen, X., Zhang, C., Zhang, G., Xu, Z., 2014. Design and manufacture of customized dental implants by using reverse engineering and selective laser melting technology. J. Prosthet. Dent 112, 1088–1095. https://doi.org/10.1016/j. prosdent.2014.04.026. E1.
- Dantas, T., Madeira, S., Gasik, M., Vaz, P., Silva, F., 2021. Customized root-analogue implants: a review on outcomes from clinical trials and case reports. Materials 14, 1–14. https://doi.org/10.3390/ma14092296.
- Dantas, T.A., Carneiro Neto, J.P., Alves, J.L., Vaz, P.C.S., Silva, F.S., 2020. In silico evaluation of the stress fields on the cortical bone surrounding dental implants: comparing root-analogue and screwed implants. J. Mech. Behav. Biomed. Mater. 104, 103667. https://doi.org/10.1016/j.jmbbm.2020.103667.
- Dumont, E.R., Grosse, I.R., Slater, G.J., 2009. Requirements for comparing the performance of finite element models of biological structures. J. Theor. Biol. 256, 96–103. https://doi.org/10.1016/j.jtbi.2008.08.017.
- Elshazly, T.M., Bourauel, C., Aldesoki, M., Ghoneima, A., Abuzayda, M., Talaat, W., Talaat, S., Keilig, L., 2023a. Computer-aided finite element model for biomechanical analysis of orthodontic aligners. Clin. Oral Investig 27, 115–124. https://doi.org/ 10.1007/s00784-022-04692-7.
- Elshazly, T.M., Salvatori, D., Elattar, H., Bourauel, C., Keilig, L., 2023b. Effect of trimming line design and edge extension of orthodontic aligners on force transmission: a 3D finite element study. J. Mech. Behav. Biomed. Mater. 140, 105741. https://doi.org/10.1016/j.jmbbm.2023.105741.
- Falcinelli, C., Valente, F., Vasta, M., Traini, T., 2023. Finite element analysis in implant dentistry: state of the art and future directions. Dent. Mater. 39, 539–556. https:// doi.org/10.1016/j.dental.2023.04.002.
- Figliuzzi, M., Mangano, F., Mangano, C., 2012. A novel root analogue dental implant using CT scan and CAD/CAM: selective laser melting technology. Int. J. Oral Maxillofac. Surg. 41, 858–862. https://doi.org/10.1016/j.ijom.2012.01.014.
- Figliuzzi, M.M., Aiello, D., Rengo, C., Parentela, L., Mangano, C., 2022. 10-Year evaluation of the first root analogue implant on humans, made using a CT scan, CAD/CAM and DMLS. Biomimetics 7, 1–7. https://doi.org/10.3390/biomimetics7010032.
- Fiorillo, L., Milone, D., D'Andrea, D., Santonocito, D., Risitano, G., Cervino, G., Cicciù, M., 2022. Finite element analysis of zirconia dental implant. Prosthesis 4, 490–499. https://doi.org/10.3390/prosthesis4030040.
- Frost, H.M., 2003. Bone's Mechanostat: a 2003 update. Anat. Rec. Part A Discov. Mol. Cell. Evol. Biol. 275. 1081–1101. https://doi.org/10.1002/ar.a.10119.
- Gattinger, J., Bullemer, C.N., Harrysson, O.L.A., 2016. Patient specific root-analogue dental implants additive manufacturing and finite element analysis. Curr. Dir. Biomed. Eng. 2, 101–104. https://doi.org/10.1515/cdbme-2016-0025.
- Heimes, D., Becker, P., Pabst, A., Smeets, R., Kraus, A., Hartmann, A., Sagheb, K., Kämmerer, P.W., 2023. How does dental implant macrogeometry affect primary implant stability? A narrative review. Int. J. Implant Dent. 9. https://doi.org/ 10.1186/s40729-023-00485-z.
- Hodosh, M., Povar, M., Shklar, G., 1969. The dental polymer implant concept.
  J. Prosthet. Dent 22, 371–380. https://doi.org/10.1016/0022-3913(69)90200-5.
- Ivanova, V., Chenchev, I., Zlatev, S., Mijiritsky, E., 2021. Correlation between primary, secondary stability, bone density, percentage of vital bone formation and implant size. Int. J. Environ. Res. Publ. Health 18. https://doi.org/10.3390/ijerph18136994.
- Javed, F., Ahmed, H., Crespi, R., Romanos, G., 2013. Role of primary stability for successful osseointegration of dental implants: factors of influence and evaluation. Interv. Med. Appl. Sci. 5, 162–167. https://doi.org/10.1556/IMAS.5.2013.4.3.
- Keilig, L., Bourauel, C., Grüner, M., Hültenschmidt, R., Bayer, S., Utz, K.H., Stark, H., 2004. Aufbau und Erprobung eines neuartigen Meßsystems für die dentale Biomechanik Meßprinzip und Beispielmessungen des Hexapod-Meß-Systems. Biomed. Tech. 49, 208–215. https://doi.org/10.1515/BMT.2004.039.
- Koh, R.U., Rudek, I., Wang, H.L., 2010. Immediate implant placement: positives and negatives. Implant Dent. 19, 98–108. https://doi.org/10.1097/ ID.0b013e3181d47eaf.
- Lundgren, D., Rylander, H., Anderssong, M., Johansson, C., Albrektsson, T., 1992.
  Healing-in of root analogue titanium implants placed in extraction sockets. An experimental study in the beagle dog. Clin. Oral Implants Res. 3, 136–144. https://doi.org/10.1034/j.1600-0501.1992.030306.x.
- Maminskas, J., Puisys, A., Kuoppala, R., Raustia, A., Juodzbalys, G., 2016. The prosthetic influence and biomechanics on peri-implant strain: a systematic literature review of finite element studies. J. Oral Maxillofac. Res. 7, e4. https://doi.org/10.5037/ jomr.2016.7304.
- Miri, R., Shirzadeh, A., Kermani, H., Khajavi, A., 2017. Relationship and changes of primary and secondary stability in dental implants: a review. Int. J. Contemp. Dent. Med. Rev. 6. https://doi.org/10.15713/ins.ijcdmr.112.
- Moin, D., Hassan, B., Wismeijer, D., 2018. Immediate nonsubmerged custom root analog implants: a prospective pilot clinical study. Int. J. Oral Maxillofac. Implants 33, e37–e44. https://doi.org/10.11607/jomi.6048.
- Moin, D.A., Hassan, B., Mercelis, P., Wismeijer, D., 2013. Designing a novel dental root analogue implant using cone beam computed tomography and CAD/CAM technology. Clin. Oral Implants Res. 24, 25–27. https://doi.org/10.1111/j.1600-0501.2011.02359.x.
- Nimmawitt, P., Aliyu, A.A.A., Lohwongwatana, B., Arunjaroensuk, S., Puncreobutr, C., Mattheos, N., Pimkhaokham, A., 2022. Understanding the stress distribution on anatomic customized root-analog dental implant at bone-implant interface for different bone densities. Materials 15. https://doi.org/10.3390/ma15186379.
- Pessanha-Andrade, M., Sordi, M.B., Henriques, B., Silva, F.S., Teughels, W., Souza, J.C. M., 2018. Custom-made root-analogue zirconia implants: a scoping review on mechanical and biological benefits. J. Biomed. Mater. Res. Part B Appl. Biomater. 106, 2888–2900. https://doi.org/10.1002/jbm.b.34147.

- Regish, K.M., Sharma, D., Prithviraj, D.R., 2013. An overview of immediate root analogue zirconia implants. J. Oral Implantol. https://doi.org/10.1563/AAID-JOI-D-10.00208
- Saeidi Pour, R., Freitas Rafael, C., Engler, M.L.P.D., Edelhoff, D., Klaus, G., Prandtner, O., Berthold, M., Liebermann, A., 2019. Historical development of root analogue implants: a review of published papers. Br. J. Oral Maxillofac. Surg. 57, 496–504. https://doi.org/10.1016/j.bjoms.2019.01.021.
- Sennerby, L., Meredith, N., 2008. Implant stability measurements using resonance frequency analysis: biological and biomechanical aspects and clinical implications. Periodontol 2000 (47), 51–66. https://doi.org/10.1111/j.1600-0757.2008.00267.x.
- Szmukler-Moncler, S., Piattelli, A., Favero, G.A., Dubruille, J.H., 2000. Considerations preliminary to the application of early and immediate loading protocols in dental implantology. Clin. Oral Implants Res. 11, 12–25. https://doi.org/10.1034/j.1600-0501.2000.011001012.x.
- Tobar-Reyes, J., Andueza-Castro, L., Jiménez-Silva, A., Bustamante-Plaza, R., Carvajal-Herrera, J., 2021. Micromotion analysis of immediately loaded implants with

- Titanium and Cobalt-Chrome superstructures. 3D finite element analysis. Clin. Exp. Dent. Res. 7, 581–590. https://doi.org/10.1002/cre2.365.
- Tribst, J.P.M., Dal Piva, A.M. de O., Blom, E.J., Kleverlaan, C.J., Feilzer, A.J., 2024. Dental biomechanics of root-analog implants in different bone types. J. Prosthet. Dent 131, 905–915. https://doi.org/10.1016/j.prosdent.2022.10.005.
- Vayron, R., Nguyen, V.H., Lecuelle, B., Lomami, H.A., Meningaud, J.P., Bosc, R., Haiat, G., 2018. Comparison of resonance frequency analysis and of quantitative ultrasound to assess dental implant osseointegration. Sensors 18. https://doi.org/ 10.3390/s18051397.
- Wang, J.Q., Zhang, Y., Pang, M., Wang, Y.Q., Yuan, J., Peng, H., Zhang, W., Dai, L., Li, H. W., 2022. Biomechanical comparison of six different root-analog implants and the conventional morse taper implant by finite element analysis. Front. Genet. 13, 1–11. https://doi.org/10.3389/fgene.2022.915679.
- Winter, W., Klein, D., Karl, M., 2013. Micromotion of dental implants: basic mechanical considerations. J. Med. Eng. 2013, 1–9. https://doi.org/10.1155/2013/265412.

## 4. Discussion with References

## 4.1 Discussion

Recent research on RAIs has shown promising long-term outcomes, with survival rates between 90 % and 95 % over follow-up periods exceeding one year (Böse et al., 2020; Figliuzzi et al., 2022). Advances in CAD/CAM and manufacturing technologies have enabled the production of RAIs with high stability and minimal marginal bone loss, supporting peri-implant tissue health. However, the available literature remains limited (Dantas et al., 2021). The aim of this study was to expand the understanding of RAIs by evaluating the accuracy of titanium and zirconia multi-rooted RAIs fabricated using additive and subtractive methods, assessing their micromotion experimentally, and developing a validated finite element model to analyse their biomechanical behaviour.

To replicate the clinical workflow of RAI placement, the implants were designed based on the natural root morphology of tooth 47 using CBCT data acquisition and CAD software (Aldesoki et al., 2023; Westover, 2019). The selection of a multi-rooted tooth enabled an in-depth evaluation of accuracy in the furcation area, a critical region that has not been extensively investigated in previous studies (Moin et al., 2014). Titanium and zirconia were chosen as implant materials due to their well-established clinical use and biomechanical properties (Dantas et al., 2021; Tribst et al., 2024). Titanium is widely used for its high strength and durability, while zirconia offers superior aesthetics, excellent biocompatibility, and lower bacterial adhesion (Niinomi, 2008; van Oers and Feilzer, 2015).

The accuracy assessment in this study is critical for ensuring the primary stability of RAIs, which relies on a precise fit between the implant and the extraction socket, unlike conventional TIs that achieve stability by extending beyond the alveolus (Lioubavina-Hack et al., 2006; Moin et al., 2014; Pirker et al., 2011). Any discrepancy in fit can compromise bone-implant contact, reducing primary stability and increasing the risk of failure (Moin et al., 2014). The RMS deviations observed ranged from 21.0 to 32.8  $\mu$ m for precision and 66.4 to 164.3  $\mu$ m for trueness, aligning with clinically acceptable thresholds for fixed and implant prosthodontics, which range from 50 to 150  $\mu$ m (Etemad-Shahidi et al., 2020; Schönherr et al., 2020). Notably, PZ demonstrated the highest precision among all tested groups, confirming previous findings by Marcel et al. (Marcel et al., 2020) that additive

manufacturing provides superior repeatability. Conversely, MZ exhibited the highest trueness, closely matching the reference CAD file, a result consistent with the study by Lerner et al. (Lerner et al., 2021). These findings highlight the trade-offs between additive and subtractive manufacturing methods, reinforcing the importance of selecting the appropriate fabrication technique based on clinical requirements.

Implant stability is a crucial determinant of successful osseointegration, and various methods such as Periotest® and resonance frequency analysis have been employed to assess it (Ivanova et al., 2021). In this study, micromotion was used as an indicator of implant stability by analysing the displacement of RAIs and TIs under controlled loading conditions (Hasan et al., 2017; Wilhelm et al., 2014). The results demonstrated no statistically significant difference in displacement along the Z-axis between RAIs and TIs, suggesting comparable primary stability between the two implant types. These findings align with Gattinger et al. (2016), who reported similar micromotion between RAIs and conventional implants in a finite element analysis study. However, total displacement was significantly higher in the RAI group than in the TI group (p < 0.05), with RAIs exhibiting increased micromotion along the X and Y axes, while TIs primarily displaced along the Z-axis. This discrepancy is likely due to the anatomical shape of RAIs, characterized by asymmetrical mesial and distal roots. Importantly, the mean micromotion values for RAIs were approximately 48 µm along the Z-axis and 96 µm in total displacement, remaining well below the 150 µm threshold considered critical for osseointegration (Szmukler-Moncler et al., 2000; Winter et al., 2013). These results indicate that despite their increased multidirectional micromotion, RAIs maintain an acceptable range of stability for successful clinical application.

FEA is an effective method for evaluating stress distribution at the bone-implant interface during mastication (Chang et al., 2018; Maminskas et al., 2016). In this study, oblique loading generated significantly higher equivalent stress than axial loading, with 4.5 times more stress for TIs and 3.5 times more for RAIs. RAIs demonstrated a more uniform stress distribution and nearly three times lower equivalent stress than TIs, attributed to their larger surface area and multirooted design (Dantas et al., 2020; Tribst et al., 2024; Wang et al., 2022). Microstrain values for both implants remained within the physiological range under axial loading. However, under oblique loading, TIs showed pathological microstrain

levels, aligning with a previous study by Dantas et al. (2020). In accordance with the findings of Gattinger et al. (2016) and Dantas et al. (2020), the present study demonstrates that RAIs exhibit enhanced primary and secondary stability. This could be attributed to their anatomical design and increased surface area in comparison to TIs (Heimes et al., 2023; Javed et al., 2013).

## 4.2 Conclusions

The manufacturing process significantly influenced the accuracy of RAIs, with 3D-printed zirconia demonstrating the highest precision and milled zirconia showing the greatest trueness. Biomechanically, RAIs exhibited micromotion within physiological limits, indicating their potential for successful osseointegration. However, their performance can be less predictable due to varying anatomical designs. FEA confirmed superior stress distribution and greater stability of RAIs over conventional threaded implants. These findings highlight RAIs as a promising alternative to traditional implants, combining high accuracy, stability, and favourable biomechanical properties. Nonetheless, further research is needed to optimize implant designs and validate long-term clinical outcomes.

## 4.3 References

Aldesoki M, Keilig L, Dörsam I, Evers-Dietze B, Elshazly TM, Bourauel C. Trueness and precision of milled and 3D printed root-analogue implants: A comparative in vitro study. J Dent 2023; 130: 104425.

Böse MWH, Hildebrand D, Beuer F, Wesemann C, Schwerdtner P, Pieralli S, Spies BC. Clinical outcomes of root-analogue implants restored with single crowns or fixed dental prostheses: A retrospective case series. J Clin Med 2020; 9: 1–19.

Chang Y, Tambe AA, Maeda Y, Wada M, Gonda T. Finite element analysis of dental implants with validation: To what extent can we expect the model to predict biological phenomena? A literature review and proposal for classification of a validation process. Int J Implant Dent 2018; 4.

Dantas TA, Carneiro Neto JP, Alves JL, Vaz PCS, Silva FS. In silico evaluation of the stress fields on the cortical bone surrounding dental implants: Comparing root-analogue and screwed implants. J Mech Behav Biomed Mater 2020; 104: 103667.

Dantas T, Madeira S, Gasik M, Vaz P, Silva F. Customized root-analogue implants: A review on outcomes from clinical trials and case reports. Materials (Basel) 2021; 14: 1–14. Etemad-Shahidi Y, Qallandar OB, Evenden J, Alifui-Segbaya F, Ahmed KE. Accuracy of 3-dimensionally printed full-arch dental models: A systematic review. J Clin Med 2020; 9: 1–18.

Figliuzzi MM, Aiello D, Rengo C, Parentela L, Mangano C. 10-year evaluation of the first root-analogue implant on humans, made using a CT scan, CAD/CAM and DMLS. Biomimetics 2022; 7: 1–7.

Gattinger J, Bullemer CN, Harrysson OLA. Patient-specific root-analogue dental implants – Additive manufacturing and finite element analysis. Curr Dir Biomed Eng 2016; 2: 101–104.

Hasan I, Heinemann F, Schwegmann M, Keilig L, Stark H, Bourauel C. Experimental investigation of commercial small diameter dental implants in porcine mandibular segments. Biomed Tech 2017; 62: 103–108.

Heimes D, Becker P, Pabst A, Smeets R, Kraus A, Hartmann A, Sagheb K, Kämmerer PW. How does dental implant macrogeometry affect primary implant stability? A narrative review. Int J Implant Dent 2023; 9: 1–10.

Ivanova V, Chenchev I, Zlatev S, Mijiritsky E. Correlation between primary, secondary stability, bone density, percentage of vital bone formation and implant size. Int J Environ Res Public Health 2021; 18: 1–9.

Javed F, Ahmed H, Crespi R, Romanos G. Role of primary stability for successful osseointegration of dental implants: Factors of influence and evaluation. Interv Med Appl Sci 2013; 5: 162–167. Lerner H, Nagy K, Pranno N, Zarone F, Admakin O, Mangano F. Trueness and precision of 3D-printed versus milled monolithic zirconia crowns: An in vitro study. J Dent 2021; 113: 103792.

Lioubavina-Hack N, Lang NP, Karring T. Significance of primary stability for osseointegration of dental implants. Clin Oral Implants Res 2006; 17: 244–250.

Maminskas J, Puisys A, Kuoppala R, Raustia A, Juodzbalys G. The Prosthetic Influence and Biomechanics on Peri-Implant Strain: A Systematic Literature Review of Finite Element Studies. J Oral Maxillofac Res 2016; 7: e4.

Marcel R, Reinhard H, Andreas K. Accuracy of CAD/CAM-fabricated bite splints: Milling vs 3D printing. Clin Oral Investig 2020; 24: 4607–4615.

Moin DA, Hassan B, Parsa A, Mercelis P, Wismeijer D. Accuracy of preemptively constructed, Cone Beam CT-, and CAD/CAM technology-based, individual Root Analogue Implant technique: An in vitro pilot investigation. Clin Oral Implants Res 2014; 25: 598–602.

Niinomi M. Biologically and mechanically biocompatible titanium alloys. Mater Trans 2008; 49: 2170–2178.

van Oers RFM, Feilzer AJ. Abutment-to-fixture load transfer and peri-implant bone stress. Am J Dent 2015; 28: 247–250.

Pirker W, Wiedemann D, Lidauer A, Kocher AA. Immediate, single stage, truly anatomic zirconia implant in lower molar replacement: A case report with 2.5 years follow-up. Int J Oral Maxillofac Surg 2011; 40: 212–216.

Schönherr JA, Baumgartner S, Hartmann M, Stampfl J. Stereolithographic additive manufacturing of high precision glass ceramic parts. Materials (Basel) 2020; 13: 1–9.

Szmukler-Moncler S, Piattelli A, Favero GA, Dubruille JH. Considerations preliminary to the application of early and immediate loading protocols in dental implantology. Clin Oral Implants Res 2000; 11: 12–25.

Tribst JPM, Dal Piva AM de O, Blom EJ, Kleverlaan CJ, Feilzer AJ. Dental biomechanics of root-analog implants in different bone types. J Prosthet Dent 2024; 131: 905–915. Wang JQ, Zhang Y, Pang M, Wang YQ, Yuan J, Peng H, Zhang W, Dai L, Li HW. Biomechanical Comparison of Six Different Root-Analog Implants and the Conventional Morse Taper Implant by Finite Element Analysis. Front Genet 2022; 13: 1–11.

Westover B. Three-Dimensional Custom-Root Replicate Tooth Dental Implants. Oral Maxillofac Surg Clin North Am 2019; 31: 489–496.

Wilhelm R, Hasan I, Keilig L, Heinemann F, Stark H, Bourauel C. Biomechanical investigations of the secondary stability of commercial short dental implants in porcine ribs. Biomed Tech 2014; 59: 507–513.

Winter W, Klein D, Karl M. Micromotion of Dental Implants: Basic Mechanical Considerations. J Med Eng 2013; 2013: 1–9.

# 5. Acknowledgements

I sincerely appreciate the invaluable support, expertise, and mentorship of Prof. Dr. rer. nat. Christoph Bourauel throughout my PhD journey. His openness to innovation and willingness to explore new ideas have been instrumental in shaping my research and academic development. I am truly fortunate to have had his guidance.

I would also like to extend my gratitude to Dr. rer. nat. Ludger Keilig for his unwavering support, collaboration, and valuable insights, which have greatly contributed to my work.

Lastly, my heartfelt thanks go to my colleagues at the Oral Technology lab, whose support, teamwork, and friendship have made this experience both enriching and memorable.